SIAM J. SCI. COMPUT.
Vol. 18, No. 6, pp. 1612–1656, November 1997

006

ARTIFICIAL BOUNDARY CONDITIONS FOR COMPUTATION OF OSCILLATING EXTERNAL FLOWS*

S. V. TSYNKOV†

Abstract. In this paper, we propose a new technique for the numerical treatment of external flow problems with oscillatory behavior of the solution in time. Specifically, we consider the case of unbounded compressible viscous plane flow past a finite body (airfoil). Oscillations of the flow in time may be caused, for example, by the time-periodic injection of fluid into the boundary layer, which in accordance with experimental data, may essentially increase the performance of the airfoil.

To conduct the actual computations, we have to somehow restrict the original unbounded domain, that is, to introduce an artificial (external) boundary and to further consider only a finite computational domain. Consequently, we will need to formulate some artificial boundary conditions (ABCs) at the introduced external boundary. The ABCs we are aiming to obtain must meet the following fundamental requirement. *One should be able to uniquely complement the solution calculated inside the finite computational domain to its infinite exterior so that the original problem is solved within the desired accuracy.*

Our construction of such ABCs for oscillating flows is based on an essential assumption: the Navier–Stokes equations can be linearized in the far field against the free-stream background. To actually compute the ABCs, we represent the far-field solution as a Fourier series in time and then apply the difference potentials method (DPM) of V. S. Ryaben'kii.

This paper contains a general theoretical description of the algorithm for setting the DPM-based ABCs for time-periodic external flows. Based on our experience in implementing analogous ABCs for steady-state problems (a simpler case), we expect that these boundary conditions will become an effective tool for constructing robust numerical methods to calculate oscillatory flows.

Key words. oscillating flows, artificial boundary conditions, boundary equations with projections, auxiliary problem, difference potentials method

AMS subject classifications. 65N99, 76M25

PII. S1064827595291145

1. Introduction.

The numerical study of problems originally formulated on unbounded domains requires the implementation of special techniques for the "treatment of infinity" (which is necessitated by the restricted facilities of modern computers). One of the corresponding techniques is based on an artificial truncation of the original infinite domain, which implies that one must set special boundary conditions at the external (artificial) boundary of the newly formed finite computational domain. The aim of this paper is to describe the theoretical foundations for constructing such ABCs for the computation of certain unsteady external flows.

Before proceeding to the actual description of the problem, let us first define the concept of *exact ABCs*. Namely, exact ABCs are the boundary conditions that enable one to uniquely complement the solution of the "truncated problem" to the unbounded exterior of the computational domain so that the original problem is solved. The exact ABCs usually appear to be nonlocal for steady-state problems in space and for time-dependent problems in both space and time; many examples can be found, e.g., in the comprehensive reviews by Givoli [1, 2].

*Received by the editors September 1, 1995; accepted for publication (in revised form) March 12, 1996. This research was performed while the author held a National Research Council Research Associateship at NASA Langley Research Center, Hampton, VA 23681-2199.

http://www.siam.org/journals/sisc/18-6/29114.html

†School of Mathematical Sciences, Tel Aviv University, Ramat Aviv, Tel Aviv 69978, Israel (tsynkov@math.tau.ac.il).

Let us note that the problem of constructing such boundary conditions that would model (in the ideal case, equivalently replace) the solution on the exterior (far-field) part of the domain differs from another well-known problem related to setting the boundary conditions for numerical algorithms, namely, to construct such boundary conditions that would ensure well posedness of the truncated problem and stability of the integration process in time. In fact, these two formulations are not completely independent. For example, the issue of well posedness for certain classes of (local) ABCs was thoroughly investigated by Gustafsson [3, 4, 5]. On the other hand, a group of delicate questions related to the issue of long-time (i.e., asymptotic) stability is studied by Carpenter, Gottlieb, and Abarbanel [6] for some specific boundary-value problems. The issue of connections between the nonlocal boundary conditions that "model the infinity" and the boundary conditions that ensure the asymptotic stability is likely to become an interesting subject for a future investigation.

In this paper, we consider an unbounded compressible viscous flow past a finite body or configuration of bodies (e.g., single-element or multi-element airfoil). The behavior of the flow in time is assumed to be oscillatory. We must emphasize that while talking about the oscillatory time behavior we mean that some alternating (time-periodic) influence is exerted on the flow (see, e.g., experimental work by Seifert et al. [7]), and we expect that those frequencies that are connected to this influence will dominate in the solution. We subsequently assume that the latter circumstance will enable us to construct the ABCs without taking into account any other time-dependent effects. From a mathematical standpoint, this case fills an intermediate position between the steady-state and true unsteady flows.

The steady-state case is relatively simple compared to time-dependent flows. In [8], we have constructed the ABCs for calculating external viscous compressible steady-state flows. These boundary conditions are based on the concept of far-field linearization and on the application of the DPM of Ryaben'kii [9, 10, 11]. The ABCs [8] are asymptotically exact, which means they can be constructed as close to the exact ABCs as desired; therefore, the ABCs [8] turn out to be global in space. However, practical implementation of these boundary conditions is fairly easy (see [12, 13]). They were used along with the Navier–Stokes code by Swanson and Turkel [14, 15] for computing different external flows. Numerical experiments show that the global DPM-based ABCs [8] provide high accuracy of computations, as well as fast convergence of the multigrid iteration procedure to a steady state [12, 13]. The computational cost of boundary conditions [8, 12, 13] is not high in comparison with the total cost of the original procedure [14, 15]. Generally, the numerical algorithm we used for integrating the Navier–Stokes equations became more robust (in comparison with the standard procedure [14, 15] itself) if supplemented by the DPM-based ABCs [8].

Let us emphasize that the ABCs [8] were constructed specially for the steady-state problem and on the basis of stationary governing equations, independent of any specific technique for solving the stationary equations inside the computational domain. In practical computations (see [12, 13]), we use multigrid iterations [14, 15] for calculating the steady-state solutions. In doing so, we set the ABCs [8] on each iteration on the upper time level. Of course, the boundary data on the intermediate stage of the iteration procedure (i.e., until we achieve a true steady state) are not necessarily consistent with the formal "stationary" treatment of the far field. However, treating the "time-intermediate" boundary data as if it were already steady has been found effective in computational practice; see [12, 13]. We are going to use a similar idea for the time-periodic case studied below.

Note that, basically, most of the currently used ABCs methodologies, especially in the area of computational fluid dynamics, are local. As a rule, such methods are not very accurate, although they are inexpensive and easy to implement. Among the very few highly accurate nonlocal techniques, which are at the same time computationally effective, we should mention the work by Verhoff, Stookesberry, and Agrawal [16], in which the authors construct the ABCs for inviscid compressible external flow computations. The main difference between our steady-state approach [8, 12, 13] and the methodology of [16] is that we analyze viscous flows, whereas the authors of [16] consider inviscid flows. However, an interesting feature of the approach of [16] is that, though the Euler equations are linearized in the far field against the constant-pressure background, a special change of variables allows the nonlinear thermodynamic relations to be retained. This enables one to explicitly take into account entropy-wake solutions (i.e., rotational effects) that are relevant to inviscid treatment of the far field. The Fourier transform (combined with a certain iteration technique) is used in [16] to solve the far-field equations and to obtain the ABCs at the C-type artificial boundary that is composed of parabolic (inflow) and linear (outflow) segments. In [17], Verhoff and Stookesberry extend the above approach to duct problems, and in [18], Verhoff uses an analogous technique to treat O-type configurations for circular artificial boundaries.

True unsteady flows are much more complicated than steady-state ones in terms of both theoretical analysis and practical calculations. As mentioned above, the exact ABCs for unsteady problems will generally be nonlocal in both space and time. Therefore, the corresponding computational cost may appear to be rather high. This is also true for the global DPM-based boundary conditions, which can be constructed as close to the exact ones as desired (the corresponding general theory for unsteady problems can be found in the work by Ryaben'kii [19]).

However, an intermediate case of oscillatory time behavior must be less expensive in terms of required computer resources, since the global character of the ABCs in time will obviously be restricted here by the value of one period. Moreover, the theoretical analysis of this case based on the usage of the Fourier representation in time (see below) is, in principle, less complicated than the general one from [19], since in our analysis we actually reduce the time-dependent problem to a family of steady-state problems.

On the other hand, do not assume that the oscillating flow is a particular, and therefore unimportant, case. For example, experiments [7] show that the time-periodic injection of fluid into the turbulent boundary layer may noticeably increase its resistance to adverse pressure gradients without separation. This implies an essential improvement of airfoil performance, up to 60% for high (post-stall) angles of attack, according to [7]. The phenomenon was observed for different geometries (original NACA0015 airfoil, the same airfoil with the deflected flap, and some others), which leads us to believe that it may be effectively used in aircraft design. Therefore, an accurate numerical investigation of the phenomenon becomes an important issue, and an accurate procedure for setting the ABCs must be one of the principle elements of any computational algorithm used for such an investigation.

The previous example is probably not a unique one where the time-periodic treatment of flow in the far field might be relevant. In general, for the oscillatory case, we propose the following construction of ABCs. First, linearize the governing equations in the far field. Then, assuming that the time period is initially prescribed, apply the Fourier transform in time and obtain a family of steady-state problems (where

the unknowns are amplitudes). The latter problems are then treated by means of the DPM [9, 10, 11]. The central idea of the DPM-based approach is to equivalently replace the problem formulated on the domain by a certain operator equation formulated on its boundary. For each one of the above-mentioned steady-state problems (note that the family of these problems is parameterized by the frequency, i.e., by the dual Fourier variable), this replacement results in an operator equation formulated at the artificial boundary of the computational domain. (This equation connects the boundary values of the solution.) The operator involved (a projection) is somewhat analogous to the boundary pseudodifferential operators introduced by Calderon [20]. Because of the equivalence to the exterior linear problem, the aforementioned operator equation (more precisely, the entire family of these equations) can be considered the desired exact ABC (limited only by the accuracy of far-field linearization) for the problem solved inside the computational domain. In other words, this operator equation adequately takes into account the structure of the solution from outside the computational domain, which may also be called *the exact transfer of boundary conditions from infinity*; see [19].

Recall that the ABCs [8] for stationary problems were constructed irrespective of any specific way for actual computation of the steady state. Analogously, in this paper, the ABCs for the time-periodic case are constructed independent of any specific technique for integrating the Navier–Stokes equations inside the computational domain. Based on the assumption of periodicity in time, these ABCs simply close the system that is solved inside the computational domain; the closure is obtained for the time interval of one period. In practice, however, achieving a true oscillatory regime may require long-time computational runs that cover many periods. During this long-time integration, whenever we need to update the external boundary data using the ABCs (i.e., every time step; see below) we treat the flow as if it were already time-periodic (in some generalized sense; see section 3). In so doing, the boundary conditions should guarantee only the desirable far-field behavior of the solution. This behavior is actually determined by the condition that all perturbations vanish at infinity. (Note that in [8, 12, 13] we were treating the external boundary data on each iteration as already steady and requiring that the ABCs ensure the decay of the solution to the linearized problem at infinity.)

The material below is organized as follows. In section 2, we describe the basic formulations of the problems. Specifically, in section 2.1, we describe the geometric setup typical for the numerical solution of external flow problems, i.e., configurations of the finite computational domain and its infinite exterior. In this section, we also introduce the flow equations (parabolized Navier–Stokes) and linearize them in the far field against the constant free-stream background. In so doing, we obtain a coupled problem, which is nonlinear inside the finite computational domain and linear outside it. Then, assuming that the period of oscillating motion is known, we Fourier-transform the exterior linear system with respect to time and obtain an equivalent family of stationary systems. These stationary systems must be solved as a part of the solution of the aforementioned coupled problem. However, we do not solve them directly, since the corresponding domain is still infinite. Instead, we replace each of these linear stationary systems by the generalized Calderon pseudodifferential equation formulated at the external boundary of the computational domain. The exterior solution is then obtained in the form of a generalized potential; the density of the potential satisfies the aforementioned boundary equation. To calculate the generalized potential, we need a special auxiliary problem, which is first formulated on the

entire plane for the linearized thin-layer equations (Fourier-transformed in time) with a certain compactly supported right-hand side. Solvability of this auxiliary problem in the sense of tempered distributions is studied in section 2.2. Then, in section 2.3, we show how one can replace the original auxiliary problem formulated on the entire plane by the new problem formulated on some rectangle, so that the solutions of the two problems are in a certain sense close to each other.

Section 3 of this paper is devoted to numerics. In section 3.1, we introduce a finite-difference scheme that approximates the linearized thin-layer equations. Since we discretize the equations not only in space but also in time, we now get a finite (discrete) series in time instead of the original infinite Fourier series. This implies that the family of stationary systems to be solved outside the computational domain becomes finite as well. In section 3.2, we construct a difference analogue to the auxiliary problem on the rectangle, describe the numerical algorithm for its solution (referring to our previous work for some details), and briefly address our somewhat nonstandard concept of convergence for the solutions of the difference auxiliary problem. Finally, in section 3.3, we show how one uses the recently formulated difference auxiliary problem and obtains a difference analogue to the Calderon boundary pseudodifferential projection. Then, calculating the generalized difference potential, we actually compute the nonlocal DPM-based ABCs. The ABCs are first obtained in the Fourier variables and then, after implementing the inverse transform, in the physical variables as well. Finally, section 4 contains some numerical data, conclusions, and possible generalizations.

2. Basic formulations.

2.1. Governing equations and geometric setup. Let us start with the parabolized Navier–Stokes equations, which are the same as the thin-layer equations for two dimensions (see, e.g., [21] by Anderson, Tannehill, and Pletcher):

$$\frac{\partial \rho}{\partial t}+\frac{\partial \rho u}{\partial x}+\frac{\partial \rho v}{\partial y}=0, \tag{2.1}$$

$$\rho\frac{\partial u}{\partial t}+\rho u\frac{\partial u}{\partial x}+\rho v\frac{\partial u}{\partial y}+\frac{\partial p}{\partial x}=\frac{1}{\mathrm{Re}}\,\frac{\partial}{\partial y}\mu\frac{\partial u}{\partial y},$$

$$\rho\frac{\partial v}{\partial t}+\rho u\frac{\partial v}{\partial x}+\rho v\frac{\partial v}{\partial y}+\frac{\partial p}{\partial y}=\frac{1}{\mathrm{Re}}\,\frac{4}{3}\,\frac{\partial}{\partial y}\mu\frac{\partial v}{\partial y},$$

$$\rho\frac{\partial \varepsilon}{\partial t}+\rho u\frac{\partial \varepsilon}{\partial x}+\rho v\frac{\partial \varepsilon}{\partial y}+p\left(\frac{\partial u}{\partial x}+\frac{\partial v}{\partial y}\right)=\frac{1}{\mathrm{Re}}\left[\mu\left(\frac{\partial u}{\partial y}\right)^2+\frac{4}{3}\,\mu\left(\frac{\partial v}{\partial y}\right)^2+\frac{\gamma}{\mathrm{Pr}}\,\frac{\partial}{\partial y}\mu\frac{\partial \varepsilon}{\partial y}\right].$$

Here, x and y denote the Cartesian coordinates, u and v denote the Cartesian velocity projections, ρ denotes the density, p denotes the pressure, ε denotes the internal energy, μ denotes the viscosity, and γ denotes the ratio of specific heats. To derive the last equation of (2.1), we assume that the gas is perfect and that the Prandtl number $\mathrm{Pr}=\mu c_p/\kappa$ is constant (κ is the heat conduction coefficient). We denote the free-stream parameters (specifically, u_0, v_0, p_0, ρ_0, ε_0, μ_0) by the subscript "0." We additionally assume that $v_0=0$ and $u_0>0$, which does not imply any loss of generality. The system (2.1) is written in dimensionless form. The following scales were used to obtain dimensionless quantities: u_0 was used for velocity, ρ_0 for density, $\rho_0{u_0}^2$ for pressure, ${u_0}^2$ for internal energy, μ_0 for viscosity, characteristic size L (typically, airfoil chord) for all distances, and L/u_0 for time. The factor $1/\mathrm{Re}$ that multiplies

the viscous terms in (2.1) arises from the nondimensionalization; here $\mathrm{Re} = \frac{\rho_0 u_0 L}{\mu_0}$ is the Reynolds number.

Note that in our previous work [8, 12, 13] we used the full Navier–Stokes equations to construct the ABCs for steady-state problems. In this paper, we are going to use the thin-layer system (2.1). This system appears to apply quite well to the description of certain viscous flows [21], in particular, the far-field flows that we are studying hereafter. Moreover, for the thin-layer system (2.1), we can justify some results on the solvability of its linearized counterpart on R^2 (see section 2.2), which is important for the general justification of our construction of ABCs. Finally, the usage of equations (2.1) instead of the full Navier–Stokes equations saves an appreciable amount of computer resources, as will be seen from further consideration.

Let us now assume that the actual values of u, v, p, ρ, ε, μ in the far field only slightly deviate from the corresponding free-stream parameters. For dimensionless quantities, this means

$$\rho = 1 + \tilde{\rho},\ u = 1 + \tilde{u},\ v = \tilde{v},\ \mu = 1 + \tilde{\mu},\ p = \left(\gamma {M_0}^2\right)^{-1} + \tilde{p}, \tag{2.2}$$
$$\varepsilon = \left((\gamma - 1)\gamma {M_0}^2\right)^{-1} + \tilde{\varepsilon},$$

where

$$\tilde{\rho} \ll 1, \quad \tilde{u} \ll 1, \quad \tilde{v} \ll 1, \quad \tilde{\mu} \ll 1, \quad \tilde{p} \ll \left(\gamma {M_0}^2\right)^{-1},$$
$$\tilde{\varepsilon} \ll \left((\gamma - 1)\gamma {M_0}^2\right)^{-1}.$$

Here, $M_0 = u_0 \left(\gamma p_0/\rho_0\right)^{-1/2}$ is the Mach number at infinity, which is always assumed to be less than unity. By substituting (2.2) into (2.1) and retaining only the first-order terms with respect to small perturbations $\tilde{u}$, $\tilde{v}$, $\tilde{p}$, $\tilde{\rho}$, $\tilde{\varepsilon}$, $\tilde{\mu}$, we obtain the following system of linear partial differential equations with constant coefficients:

$$\mathbf{C}\frac{\partial \mathbf{u}}{\partial t} + \mathbf{D}\frac{\partial \mathbf{u}}{\partial x} + \mathbf{F}\frac{\partial \mathbf{u}}{\partial y} + \mathbf{H}\frac{\partial^2 \mathbf{u}}{\partial y^2} = \mathbf{0}, \tag{2.3a}$$

where

$$\mathbf{u} = \begin{bmatrix} u \\ v \\ p \\ \rho \end{bmatrix}, \quad \mathbf{C} = \begin{bmatrix} 0 & 0 & 0 & 1 \\ 1 & 0 & 0 & 0 \\ 0 & 1 & 0 & 0 \\ 0 & 0 & 1 & -{M_0}^{-2} \end{bmatrix}, \quad \mathbf{D} = \begin{bmatrix} 1 & 0 & 0 & 1 \\ 1 & 0 & 1 & 0 \\ 0 & 1 & 0 & 0 \\ 0 & 0 & 1 & -{M_0}^{-2} \end{bmatrix}, \tag{2.3b}$$
$$\mathbf{F} = \begin{bmatrix} 0 & 1 & 0 & 0 \\ 0 & 0 & 0 & 0 \\ 0 & 0 & 1 & 0 \\ 0 & 0 & 0 & 0 \end{bmatrix}, \quad \mathbf{H} = -\frac{1}{\mathrm{Re}} \begin{bmatrix} 0 & 0 & 0 & 0 \\ 1 & 0 & 0 & 0 \\ 0 & 4/3 & 0 & 0 \\ 0 & 0 & \gamma \mathrm{Pr}^{-1} & -\mathrm{Pr}^{-1} {M_0}^{-2} \end{bmatrix}.$$

The system (2.3) is the linearization of equations (2.1) against the free-stream background. We omit the tilde $\tilde{}$ in (2.3), since we are going to deal only with linear equations in perturbations henceforth. We also note that the equation of state $\varepsilon = \frac{1}{\gamma - 1}\frac{p}{\rho}$ (more precisely, its linearization, $\tilde{\varepsilon} = \frac{1}{\gamma-1}(\tilde{p} - \frac{1}{\gamma {M_0}^2}\tilde{\rho})$) was used to eliminate internal energy from (2.3).

We have mentioned that equations (2.3) will be used for the description of fluid motion in the far field. Let us now define a general geometric setup for the problem

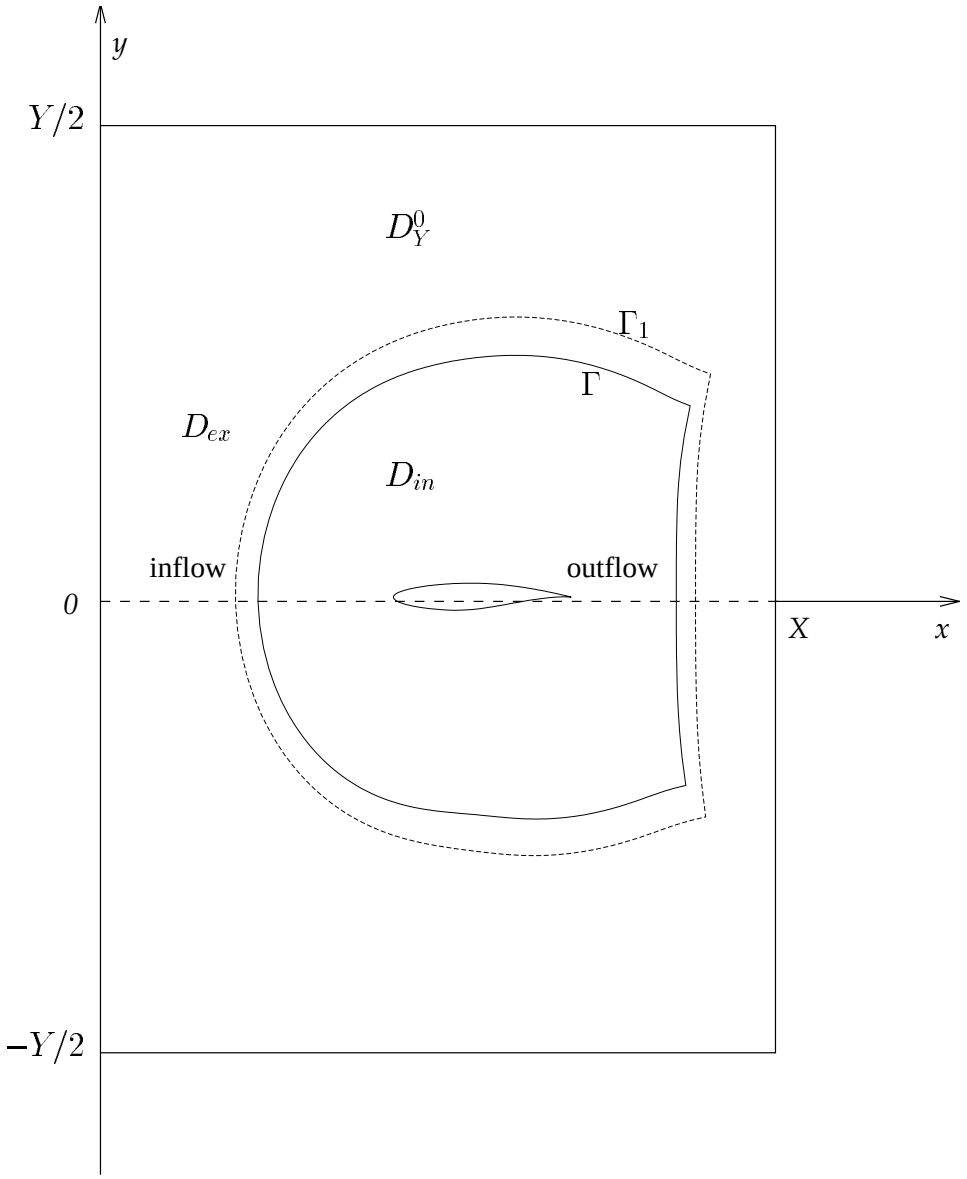

FIG. 2.1. *Configuration of domains.*

under consideration. The original Navier–Stokes equations are integrated on a grid (e.g., of the C type) generated around the airfoil; this grid covers the finite computational domain which is denoted D_{in} hereafter (see Figure 2.1). We henceforth assume that the linearization (2.3) is valid outside the computational domain D_{in}, i.e., on its complement D_{ex} (see Figure 2.1). Clearly, this assumption is true for large computational domains, i.e., far enough from the immersed body. As we approach the airfoil, the validity of linearization in D_{ex} can always be verified a posteriori, i.e., by analyzing the corresponding computational results (as done, e.g., in [12, 13] for the steady-state case).

To integrate the Navier–Stokes equations on the grid inside D_{in}, we use some finite-dimensional approximation of these equations. The actual type of the resulting discrete operator (i.e., finite-difference, finite-element, etc.) is not that important from the standpoint of constructing the ABCs; for definiteness, we assume that the Navier–Stokes equations are integrated by means of a finite-difference scheme. To begin with, we also suppose that this scheme is fully explicit in time. We may always think that we already know the solution for the time level t^l on the entire grid; in particular, $l = 0$ implies the initial data. When we advance one time step, i.e., calculate the solution for the level t^{l+1} by means of the scheme, we cannot obtain this solution for the whole grid because some nodes located near the external boundary of D_{in} will be missing. The actual location of missing nodes depends on the specific structure of the scheme stencil. For example, a typical central-difference second-order approximation to the spatial part of the Navier–Stokes operator on a structured grid requires a 3×3 stencil. Using such spatial approximation combined with an explicit integration procedure in time, we can obtain the solution on the level t^{l+1} at all nodes, except for those that belong to the outermost coordinate row of the grid (designated Γ_1 on Figure 2.1). To advance the next time step (t^{l+2}) we will have to somehow determine these missing values of the solution on the level t^{l+1}. This will be done by representing the solution to (2.3) in the form of a generalized potential for each Fourier mode. Thus, using the solution to (2.3) in D_{ex}, we close the system of difference equations inside the computational domain D_{in}; the closure we obtain is actually the desired ABCs.

In the case of implicit schemes, we also need the ABCs that will close the system of difference equations inside D_{in}. Indeed, while integrating the Navier–Stokes equations by means of an implicit scheme, one has to solve a certain discrete system on the upper time level (t^{l+1}), whereas the data from the lower time level(s) play the role of forcing terms. The above system will obviously be subdefinite unless we specify additional relations that connect the values of unknowns at the grid nodes located near the external boundary. In particular, for the previously mentioned example of a structured grid and central differences on the 3×3 spatial stencil, these additional relations, i.e., the ABCs, should connect the values of the solution at the penultimate (the curve Γ on Figure 2.1) and outermost rows of grid nodes (see also [8, 12, 13]). By including the missing relations that are provided by the ABCs into the system solved on the upper time level, we close this system and then advance the next time step.

Let us now provide an exact formulation of the problem. First, we select those nodes of the grid where the solution can no longer be determined by the scheme, but must be obtained by means of special additional relations, i.e., by means of the ABCs. We designate this set of nodes ν_1. Second, we select those nodes of the grid where we need to know the solution in order to obtain it on ν_1 with the help of the ABCs. The latter set is designated ν. Both ν and ν_1 will depend on the structure of the specific stencil. In particular, for the 3×3 stencil on a structured grid, ν and ν_1 correspond to the penultimate and outermost rows of grid nodes, respectively (see also [8, 12, 13]). Without loss of generality, we assume that the artificial boundary Γ (see Figure 2.1) is formed by the penultimate row of nodes ν, so that all nodes ν_1 that form the curve Γ_1 (see Figure 2.1) already belong to D_{ex} (i.e., to the "linear zone").

Then, we designate the time period by T. Clearly, we can further consider our problem for the time interval $[0, T]$ without loss of generality. We will also need the following brief notations: $D_{ex}^T = D_{ex} \times [0, T]$, $D_{in}^T = D_{in} \times [0, T]$, $\Gamma^T = \Gamma \times [0, T]$, and $\Gamma_1^T = \Gamma_1 \times [0, T]$. The closure of the finite-difference system in D_{in}^T, which we are looking for and which should be provided by the ABCs, is actually a set of relations

expressing $\mathbf{u}|_{\Gamma_1^T}$ in terms of some data specified on Γ^T. As previously mentioned, these relations will be based on the solution to the linearized system (2.3) in D_{ex}^T. The latter system is supplemented (on D_{ex}^T) by the periodicity condition in time:

$$\mathbf{u}|_{t=0} = \mathbf{u}|_{t=T}, \quad (x,\, y) \in D_{ex}, \tag{2.4}$$

and the free-stream condition at infinity:

$$\mathbf{u} \longrightarrow \mathbf{0}, \quad \text{as } x^2 + y^2 \longrightarrow \infty, \quad t \in [0,\, T]. \tag{2.5}$$

The choice of data on Γ^T that "drive" the ABCs is closely connected to the concept of *clear trace* delineated in [9, 10]. The question of the possible proper constructions of clear traces for (2.3) may require a special thorough investigation in addition to the general analysis from [9, 10]; such an investigation is not a direct subject of this paper. Therefore, we will not comment on this question in our further discussion; we only point out the actual construction we use. Namely, let us first represent the vector function $\mathbf{u}(x,\, y,\, t)$ in the form of a Fourier series in time for any space point $(x,\, y)$,

$$\mathbf{u}(x,\, y,\, t) = \sum_{n=-\infty}^{n=\infty} \hat{\mathbf{u}}^n(x,\, y) e^{int\frac{2\pi}{T}}, \tag{2.6}$$

where

$$\hat{\mathbf{u}}^n(x,\, y) = \frac{1}{T} \int_0^T \mathbf{u}(x,\, y,\, t) e^{-int\frac{2\pi}{T}}\, dt, \quad n = 0, \pm 1, \pm 2, \ldots. \tag{2.7}$$

Instead of considering (2.3a)–(2.4)–(2.5) on D_{ex}^T, we henceforth consider on D_{ex} the family of "stationary" systems

$$i\omega_n \mathbf{C}\hat{\mathbf{u}}^n + \mathbf{D}\frac{\partial \hat{\mathbf{u}}^n}{\partial x} + \mathbf{F}\frac{\partial \hat{\mathbf{u}}^n}{\partial y} + \mathbf{H}\frac{\partial^2 \hat{\mathbf{u}}^n}{\partial y^2} = \mathbf{0}, \quad n = 0, \pm 1, \pm 2, \ldots, \tag{2.8}$$

parameterized by the frequency $\omega_n = 2\pi n/T$, $n = 0, \pm 1, \pm 2, \ldots$, and supplemented at infinity by the boundary conditions

$$\hat{\mathbf{u}}^n(x,\, y) \longrightarrow \mathbf{0}, \quad \text{as } x^2 + y^2 \longrightarrow \infty, \quad n = 0, \pm 1, \pm 2, \ldots, \tag{2.9}$$

which directly follow from (2.5). The matrices $\mathbf{C}$, $\mathbf{D}$, $\mathbf{F}$, and $\mathbf{H}$ in the system (2.8) are the same as in (2.3b).

For each frequency ω_n, we consider the pair of functions $(\hat{\mathbf{u}}_\Gamma^n,\, \frac{\partial \hat{\mathbf{u}}_\Gamma^n}{\partial \zeta})$ specified on Γ as the data that "drive" the ABCs; here, ζ is the normal to Γ. (Note that if the interior solution is already computed by means of the scheme inside D_{in}^T, then $\hat{\mathbf{u}}_\Gamma^n$ and $\frac{\partial \hat{\mathbf{u}}_\Gamma^n}{\partial \zeta}$ are available.)

Our ultimate goal will be to provide a full classification of all those and only those functions $(\hat{\mathbf{v}}_\Gamma^n,\, \frac{\partial \hat{\mathbf{v}}_\Gamma^n}{\partial \zeta})$ that generate on D_{ex} a solution $\hat{\mathbf{u}}^n(x,\, y)$ to (2.8)–(2.9) with the trace on Γ that coincides with the "source" function itself, i.e.,

$$\left(\hat{\mathbf{u}}^n,\, \frac{\partial \hat{\mathbf{u}}^n}{\partial \zeta}\right)\Bigg|_\Gamma = \left(\hat{\mathbf{v}}_\Gamma^n,\, \frac{\partial \hat{\mathbf{v}}_\Gamma^n}{\partial \zeta}\right). \tag{2.10}$$

(More precisely, we do that in the discrete framework; see section 3.) As will be seen from further consideration, the corresponding set of functions $(\hat{\mathbf{v}}_\Gamma^n, \frac{\partial \hat{\mathbf{v}}_\Gamma^n}{\partial \zeta})$ can be described as an image of a certain boundary projection operator. In other words, these functions $(\hat{\mathbf{v}}_\Gamma^n, \frac{\partial \hat{\mathbf{v}}_\Gamma^n}{\partial \zeta})$ will satisfy some boundary operator equation with projection. (The equation of this type was mentioned in section 1 as the one equivalent to the linearized exterior problem.) Let us designate the corresponding projection operator by $\mathbf{P}_\Gamma^n$; we actually construct this operator in section 3. Then, specifying a function $(\hat{\mathbf{u}}_\Gamma^n, \frac{\partial \hat{\mathbf{u}}_\Gamma^n}{\partial \zeta})$ from inside D_{in}, we apply $\mathbf{P}_\Gamma^n$ and consider the projection $\mathbf{P}_\Gamma^n(\hat{\mathbf{u}}_\Gamma^n, \frac{\partial \hat{\mathbf{u}}_\Gamma^n}{\partial \zeta}) = (\hat{\mathbf{v}}_\Gamma^n, \frac{\partial \hat{\mathbf{v}}_\Gamma^n}{\partial \zeta})$ as the right-hand side in (2.10) for the problem (2.8)–(2.9)–(2.10). Representing the solution to (2.8)–(2.9)–(2.10) in the form of a generalized potential [9, 10, 11], we find its trace on Γ_1 (i.e., on ν_1), which in turn enables us to obtain the missing boundary relations that close the system of difference equations inside D_{in}^T. These relations, i.e., the ABCs, are derived using the inverse Fourier transform. They can be symbolically written as

$$\mathbf{u}_{\nu_1} = \left(\mathbf{P}_{ex}^n \circ \mathbf{P}_\Gamma^n \circ \mathbf{R} \left(\hat{\mathbf{u}}_\nu^n, \frac{\partial \hat{\mathbf{u}}_\nu^n}{\partial \zeta} \right) \right)^{\check{}} \Big|_{\nu_1}, \quad t \in [0, T], \tag{2.11}$$

where the operator $\mathbf{R}$ represents some (smooth) interpolation of the discrete functions along the curve Γ, and the operator $\mathbf{P}_{ex}^n$ involves the calculation of the generalized potential to solve (2.8)–(2.9)–(2.10). The specific structure of all operators from (2.11) will be delineated in section 3, where we actually construct their discrete counterparts.

Let us make a few important remarks. First, to formally close the system solved in D_{in}^T, we have to obtain additional relations between the values of the unknowns on Γ^T and on Γ_1^T. Such relations would provide ABCs that are completely independent of any specific numerical procedure employed inside D_{in}^T. However, to simplify our task and at the same time only slightly compromise the above-mentioned independence, we take into account that we almost always integrate the Navier–Stokes equations step by step in time (explicitly or implicitly). Therefore, we do not need to construct such ABCs that would connect the values of the solution at ν and at ν_1 for the entire interval $[0, T]$. In fact, it suffices to determine u, v, p, and ρ at ν_1 only for $t = T$ (i.e., at the upper time level), since for all previous moments these values have already been determined when calculating previous time steps. Moreover, the formulation (2.8)–(2.9)–(2.10), where the right-hand side from (2.10) belongs to the projection image, $(\hat{\mathbf{v}}_\Gamma^n, \frac{\partial \hat{\mathbf{v}}_\Gamma^n}{\partial \zeta}) \in \operatorname{Im} \mathbf{P}_\Gamma^n$, assumes that these data are the result of operating by $\mathbf{P}_\Gamma^n$ on the Fourier transform $(\hat{\mathbf{u}}_\Gamma^n, \frac{\partial \hat{\mathbf{u}}_\Gamma^n}{\partial \zeta})$ of some time-periodic function. However, in conducting the step-by-step integration in time, the actual data $(\mathbf{u}_\Gamma, \frac{\partial \mathbf{u}_\Gamma}{\partial \zeta})$ may not be periodic until we achieve a true oscillatory regime. Therefore, as mentioned in section 1, any time we use the ABCs we implement a certain generalized treatment of the external flow as being already time-periodic. Namely, instead of the true boundary data $(\mathbf{u}_\Gamma, \frac{\partial \mathbf{u}_\Gamma}{\partial \zeta})$ at Γ^T, we use the best approximation of this data by periodic functions in the sense of least squares. This approach will be delineated in section 3, which is devoted to numerics.

Second, to treat the problem (2.8)–(2.9)–(2.10) on D_{ex}, we will need additional truncation. Recall that we have already truncated the original infinite domain and obtained D_{in}; now we also truncate D_{ex} in order to get the new linear problem

formulated on a finite domain and, therefore, available for solution on the computer. This issue is addressed in section 2.3.

Third, we certainly will not solve (2.8)–(2.9)–(2.10) every time we need to obtain a closed system inside D_{in} (i.e., each time step). Instead, using the linearity of the problem, we will specify some basis in the space of boundary data and solve (2.8)–(2.9)–(2.10) once for each basis function. This approach will enable us to obtain the ABCs in matrix form, which is very convenient for practical computing (see also [8, 12, 13]).

Ultimately, we will deal only with the finite-difference formulations and, consequently, with the finite Fourier series (instead of the infinite series (2.6); see section 3). In so doing, the discretization in time for the linearized exterior problem in D_{ex}^T should not necessarily coincide with the one used for the Navier–Stokes scheme inside D_{in}^T. A more convenient method may be to use interpolation in time, which was previously proposed in [19].

Finally, let us mention that since we need to know the solution on Γ for the whole period T to restore the solution on ν_1, the first few time steps (until the total time reaches T) will require some special treatment. It might be based on the usage of either a larger grid or some other external boundary conditions for the initial stage of integration in time.

We now proceed to the actual construction of the operators involved in (2.11). This construction will be essentially the same for all wavenumbers n. As mentioned before, the computation of the ABCs (2.11) consists of two stages. (In practice, these two stages can be combined into one, but for the purpose of analysis it is convenient to consider them separately.) First, we apply the projection $\mathbf{P}_\Gamma^n$ to provide the proper boundary data (right-hand side of (2.10)) for the problem (2.8)–(2.9)–(2.10). Then find the solution to (2.8)–(2.9)–(2.10) in the form of a generalized potential (operator $\mathbf{P}_{ex}^n$). The computation of the generalized potential $\mathbf{P}_{ex}^n$ (and projection $\mathbf{P}_\Gamma^n$) requires solving the special *auxiliary problem (AP)*. The AP is described in sections 2.2 and 2.3 for the continuous formulation and in section 3.2 for the difference formulation. This AP is actually the main element of the DPM-based approach. The Green (i.e., inverse) operator of the AP plays in the theory of generalized potentials approximately the same role as convolution with the fundamental solution plays in classical potential theory [9, 10]. The AP is formulated on the entire plane (x, y) for the inhomogeneous counterpart of the system (2.8) with a certain compactly supported right-hand side $\hat{\mathbf{f}}^n = (\hat{f}_1^n, \hat{f}_2^n, \hat{f}_3^n, \hat{f}_4^n)$ (to be specified later on). Namely, we will need to solve the following system:

$$i\omega_n \mathbf{C}\hat{\mathbf{u}}^n + \mathbf{D}\frac{\partial \hat{\mathbf{u}}^n}{\partial x} + \mathbf{F}\frac{\partial \hat{\mathbf{u}}^n}{\partial y} + \mathbf{H}\frac{\partial^2 \hat{\mathbf{u}}^n}{\partial y^2} = \hat{\mathbf{f}}^n, \quad (x, y) \in R^2, \tag{2.12}$$

$\mathrm{supp}\hat{\mathbf{f}}^n(x, y) \subset D_{in}$, and we will require that the solution be unique in the class of functions vanishing at infinity. In other words, the system (2.12) is supplemented by the boundary condition

$$\hat{\mathbf{u}}^n(x, y) \longrightarrow \mathbf{0}, \quad \text{as } x^2 + y^2 \longrightarrow \infty, \tag{2.13}$$

which is the same as (2.9).

Once we are able to solve the AP (2.12)–(2.13), then we can properly formulate the problem (2.8)–(2.9)–(2.10) and obtain its solution in the form of a generalized potential. This is actually a very brief description of our DPM-based approach; it will

be delineated in section 3 for the discrete formulation of the problem. Now we will investigate the solvability of the AP (2.12)–(2.13).

2.2. Solvability of the linearized problem on the entire plane. We will look for the solution to (2.12)–(2.13) in the space of tempered distributions $\mathcal{G}'$ (see [22] by Hörmander or [23] by Vladimirov), which is a conjugate space to the space $\mathcal{G}$ of all infinitely smooth functions that are defined on R^2, and decrease at infinity with all their derivatives faster than any power of $(x^2+y^2)^{-1/2}$. Take the Fourier transform

$$\hat{\hat{\mathbf{u}}}^n(\xi,\eta)=\frac{1}{2\pi}\int_{-\infty}^{\infty}\int_{-\infty}^{\infty}\hat{\mathbf{u}}^n(x,y)\,e^{-i\xi x-i\eta y}dx\,dy, \tag{2.14a}$$

$$\hat{\hat{\mathbf{f}}}^n(\xi,\eta)=\frac{1}{2\pi}\int_{-\infty}^{\infty}\int_{-\infty}^{\infty}\hat{\mathbf{f}}^n(x,y)\,e^{-i\xi x-i\eta y}dx\,dy \tag{2.14b}$$

of both sides of (2.12), and represent the result in the form of a matrix equation

$$\mathbf{Q}\hat{\hat{\mathbf{u}}}=\hat{\hat{\mathbf{f}}}. \tag{2.15}$$

Note that in the system (2.15) and henceforth in this subsection, we drop the superscript n to simplify the notations. The symbol $\mathbf{Q}$ from (2.15) is given by

$$\mathbf{Q}=i\omega\mathbf{C}+i\xi\mathbf{D}+i\eta\mathbf{F}-\eta^2\mathbf{H} \tag{2.16}$$

$$=\begin{bmatrix} i\xi & i\eta & 0 & i(\omega+\xi) \\ i(\omega+\xi)+\frac{\eta^2}{\mathrm{Re}} & 0 & i\xi & 0 \\ 0 & i(\omega+\xi)+\frac{4}{3}\frac{\eta^2}{\mathrm{Re}} & i\eta & 0 \\ 0 & 0 & i(\omega+\xi)+\frac{\gamma\eta^2}{\mathrm{Re\,Pr}} & -\frac{i}{M_0{}^2}(\omega+\xi)-\frac{\eta^2}{\mathrm{Re\,Pr}\,M_0{}^2} \end{bmatrix}.$$

We first show that the system (2.15) is solvable in $\mathcal{G}'$. For the time being, we do not need any restrictive assumptions regarding $\hat{\mathbf{f}}$; as previously mentioned, $\hat{\mathbf{f}}$ is compactly supported, $\mathrm{supp}\hat{\mathbf{f}}\subset D_{in}$, and without loss of generality, we may think that $\hat{\mathbf{f}}$ is absolutely integrable on R^2 ($\hat{\mathbf{f}}\in L^1(R^2)$). Then, its Fourier transform $\hat{\hat{\mathbf{f}}}$ is bounded and continuous on R^2; consequently, if we formally write down the solution to (2.15) as

$$\hat{\hat{\mathbf{u}}}=\mathbf{Q}^{-1}\hat{\hat{\mathbf{f}}}, \tag{2.17}$$

then the properties of the right-hand side in (2.17) are fully determined by the inverse symbol $\mathbf{Q}^{-1}$. Indeed, it is well known [23] that if the right-hand side of (2.17) is locally absolutely integrable on R^2, then it defines the tempered distribution, i.e., the generalized function from $\mathcal{G}'$. The latter will coincide (in the sense of distributions) with the classical function $\mathbf{Q}^{-1}(\xi,\eta)\hat{\hat{\mathbf{f}}}(\xi,\eta)$ everywhere on R^2, except for the set of singularities of $\mathbf{Q}^{-1}(\xi,\eta)\hat{\hat{\mathbf{f}}}(\xi,\eta)$ (if any). Since in our case the function $\hat{\hat{\mathbf{f}}}(\xi,\eta)$ is continuous and bounded on R^2, then it suffices to determine whether the function $\mathbf{Q}^{-1}(\xi,\eta)$ belongs to $L^1_{loc}(R^2)$.

To do this, we have to find all singularities of $\mathbf{Q}^{-1}(\xi,\,\eta)$. Calculating the determinant of $\mathbf{Q}(\xi,\,\eta)$, we obtain

$$
\begin{aligned}
Q(\xi,\,\eta) = \Bigg[& -(\omega+\xi)^4 + \frac{(\omega+\xi)^2}{{M_0}^2}(\xi^2+\eta^2) \\
& + \frac{(\omega+\xi)^2\eta^4}{\mathrm{Re}^2}\left(\frac{4}{3}+\frac{7}{3}\frac{\gamma}{\mathrm{Pr}}\right) - \frac{4}{3}\frac{\xi^2\eta^4}{{M_0}^2\mathrm{Pr}\,\mathrm{Re}^2} - \frac{\eta^6}{{M_0}^2\mathrm{Pr}\,\mathrm{Re}^2}\Bigg] \\
& + i\Bigg[\frac{(\omega+\xi)^3\eta^2}{\mathrm{Re}}\left(\frac{7}{3}+\frac{\gamma}{\mathrm{Pr}}\right) - \frac{(\omega+\xi)\xi^2\eta^2}{{M_0}^2\mathrm{Re}}\left(\frac{4}{3}+\frac{1}{\mathrm{Pr}}\right) \\
& - \frac{(\omega+\xi)\eta^4}{{M_0}^2\mathrm{Re}}\left(1+\frac{1}{\mathrm{Pr}}\right) - \frac{4}{3}\gamma\frac{(\omega+\xi)\eta^6}{\mathrm{Pr}\,\mathrm{Re}^3}\Bigg].
\end{aligned}
\tag{2.18}
$$

Here, ξ, η are the variables and ω, M_0, Re, Pr, γ are parameters. We emphasize that both variables ξ and η are supposed to be real (see (2.14)); however, the coefficients of $Q(\xi,\,\eta)$ are, generally speaking, complex. Thus, to find singular points of the symbol (2.16), one has to find the real roots of $Q(\xi,\,\eta)$ (see (2.18)), which actually implies finding common real roots of two polynomials, $\Re Q(\xi,\,\eta)$ and $\Im Q(\xi,\,\eta)$. First, the point $\xi = -\omega$, $\eta = 0$ is clearly one of such common roots. Then, we note that $\Im Q(\xi,\,\eta)$ turns into zero on the two entire straight lines, $\xi = -\omega$ and $\eta = 0$. Moreover, $\Re Q(\xi,\,\eta)$ has no other roots on the line $\xi = -\omega$, except for $\eta = 0$. Further, substituting $\eta = 0$ into the equation $\Re Q(\xi,\,\eta) = 0$ (see (2.18)) and assuming that $\xi \neq -\omega$, we find the following two roots of $\Re Q(\xi,\,\eta) = 0$ that belong to the line $\eta = 0$: $\xi_1 = \frac{\omega M_0}{1-M_0}$, $\xi_2 = -\frac{\omega M_0}{1+M_0}$. We also observe that if $\omega = 0$ (which corresponds to the steady-state flows), then all three roots, $(-\omega,\,0)$, $(\frac{\omega M_0}{1-M_0},\,0)$, and $(-\frac{\omega M_0}{1+M_0},\,0)$, merge into one.

In an attempt to find other real roots (if any) of $Q(\xi,\,\eta)$ (see (2.18)), we divide the equation $\Im Q(\xi,\,\eta) = 0$ by $(\omega+\xi)\eta^2/\mathrm{Re}$. (It is possible, since we have already proven that no other zeros exist on the two lines $\xi = -\omega$ and $\eta = 0$ except for those already found.) The resulting equation,

$$
\begin{aligned}
& (\omega+\xi)^2\left(\frac{7}{3}+\frac{\gamma}{\mathrm{Pr}}\right) - \frac{\xi^2}{{M_0}^2}\left(\frac{4}{3}+\frac{1}{\mathrm{Pr}}\right) \\
& - \frac{\eta^2}{{M_0}^2}\left(1+\frac{1}{\mathrm{Pr}}\right) - \frac{4}{3}\gamma\frac{\eta^4}{\mathrm{Pr}\,\mathrm{Re}^2} = 0,
\end{aligned}
\tag{2.19}
$$

is of the fourth order, and taking into account that the equation $\Re Q(\xi,\,\eta) = 0$ (see (2.18)) is of the sixth order, we conclude that the polynomial $Q(\xi,\,\eta)$ may have no more than a finite number of isolated real roots in total (three of which have already been found). We emphasize here that this property (finite number of isolated real roots) presents an essential difference between the problem under investigation and classical acoustics problems in which the viscous terms in the governing equations are usually neglected. Namely, for the acoustics equations (i.e., linearized Euler equations), the singular points of the symbol are no longer isolated. They usually form a curve on the plane R^2. This circumstance may cause noticeable difficulties when justifying uniqueness of the solution. The difficulties are similar to those that arise in studying the Helmholtz equation, which may be referred to as describing acoustics in the stationary medium. We do not deal with Helmholtz-like equations in this paper; we only note that contrary to the acoustics case the system (2.12) is presumably

easier from the standpoint of analyzing the uniqueness, since the corresponding proof appears elementary (see Proposition 2.4 below).

Equation (2.19) is of the second order with respect to ξ. Therefore, we can resolve it for each η and obtain explicit function(s) $\xi_{\Im} = \xi_{\Im}(\eta)$. Because we are interested only in real solutions, we have to consider a few different cases.

First, we assume that $\omega \neq 0$. Then, we rewrite (2.19) as

$$\xi^2\left(\frac{7}{3}+\frac{\gamma}{\mathrm{Pr}}-\frac{1}{{M_0}^2}\left(\frac{4}{3}+\frac{1}{\mathrm{Pr}}\right)\right)+2\omega\xi\left(\frac{7}{3}+\frac{\gamma}{\mathrm{Pr}}\right)+\omega^2\left(\frac{7}{3}+\frac{\gamma}{\mathrm{Pr}}\right) - \frac{\eta^2}{{M_0}^2}\left(1+\frac{1}{\mathrm{Pr}}\right)-\frac{4}{3}\gamma\frac{\eta^4}{\mathrm{Pr}\,\mathrm{Re}^2}=0 \tag{2.20}$$

and observe that if ${M_0}^2 = (\frac{4}{3}+\frac{1}{\mathrm{Pr}})(\frac{7}{3}+\frac{\gamma}{\mathrm{Pr}})^{-1}$, then equation (2.20) degenerates and therefore has a unique real solution $\xi_{\Im}^{(0)} = \xi_{\Im}^{(0)}(\eta)$ for any η. If ${M_0}^2 > (\frac{4}{3}+\frac{1}{\mathrm{Pr}})\cdot(\frac{7}{3}+\frac{\gamma}{\mathrm{Pr}})^{-1}$, then we can easily make sure that the discriminant

$$D = 4\omega^2\left(\frac{7}{3}+\frac{\gamma}{\mathrm{Pr}}\right)^2-4\left(\frac{7}{3}+\frac{\gamma}{\mathrm{Pr}}-\frac{1}{{M_0}^2}\left(\frac{4}{3}+\frac{1}{\mathrm{Pr}}\right)\right) \cdot\left(\omega^2\left(\frac{7}{3}+\frac{\gamma}{\mathrm{Pr}}\right)-\frac{\eta^2}{{M_0}^2}\left(1+\frac{1}{\mathrm{Pr}}\right)-\frac{4}{3}\gamma\frac{\eta^4}{\mathrm{Pr}\,\mathrm{Re}^2}\right) \tag{2.21}$$

is always positive, which means that equation (2.19) has two different real solutions, $\xi_{\Im}^{(1)} = \xi_{\Im}^{(1)}(\eta)$ and $\xi_{\Im}^{(2)} = \xi_{\Im}^{(2)}(\eta)$, for any η. If ${M_0}^2 < (\frac{4}{3}+\frac{1}{\mathrm{Pr}})(\frac{7}{3}+\frac{\gamma}{\mathrm{Pr}})^{-1}$, then the condition $D \geq 0$ (see (2.21)) imposes certain restrictions on η. Namely, we have

$$-\left[\frac{3\mathrm{Pr}\,\mathrm{Re}^2}{8\gamma}\left(-\frac{1}{{M_0}^2}\left(1+\frac{1}{\mathrm{Pr}}\right)+\sqrt{D_1}\right)\right]^{1/2} \leq \eta \leq \left[\frac{3\mathrm{Pr}\,\mathrm{Re}^2}{8\gamma}\left(-\frac{1}{{M_0}^2}\left(1+\frac{1}{\mathrm{Pr}}\right)+\sqrt{D_1}\right)\right]^{1/2}, \tag{2.22}$$

where

$$D_1 = \frac{1}{{M_0}^4}\left(1+\frac{1}{\mathrm{Pr}}\right)^2-\frac{16}{3}\frac{\gamma\omega^2}{\mathrm{Pr}\,\mathrm{Re}^2{M_0}^2}\left(\frac{7}{3}+\frac{\gamma}{\mathrm{Pr}}\right)\left(\frac{4}{3}+\frac{1}{\mathrm{Pr}}\right) \cdot\left(\frac{7}{3}+\frac{\gamma}{\mathrm{Pr}}-\frac{1}{{M_0}^2}\left(\frac{4}{3}+\frac{1}{\mathrm{Pr}}\right)\right)^{-1}.$$

Therefore, in this case the real solutions to (2.19), $\xi_{\Im}^{(1)} = \xi_{\Im}^{(1)}(\eta)$ and $\xi_{\Im}^{(2)} = \xi_{\Im}^{(2)}(\eta)$, exist only for η within the above range; see inequality (2.22).

Now consider the case $\omega = 0$ (which corresponds to the steady-state problem). From (2.19), we easily derive

$$\xi^2\left(\frac{7}{3}+\frac{\gamma}{\mathrm{Pr}}-\frac{1}{{M_0}^2}\left(\frac{4}{3}+\frac{1}{\mathrm{Pr}}\right)\right)=\frac{\eta^2}{{M_0}^2}\left(1+\frac{1}{\mathrm{Pr}}\right)+\frac{4}{3}\gamma\frac{\eta^4}{\mathrm{Pr}\,\mathrm{Re}^2}. \tag{2.23}$$

Clearly, equation (2.23) has real solutions, $\xi_{\Im}^{(1)} = \xi_{\Im}^{(1)}(\eta)$ and $\xi_{\Im}^{(2)} = \xi_{\Im}^{(2)}(\eta)$, only for ${M_0}^2 > (\frac{4}{3}+\frac{1}{\mathrm{Pr}})(\frac{7}{3}+\frac{\gamma}{\mathrm{Pr}})^{-1}$. Otherwise, we conclude that the equation $\Im Q(\xi, \eta) = 0$

for $\omega = 0$ has no other real roots except for $\xi = 0$, $\eta = 0$, and therefore, the same is true for the equation $Q(\xi, \eta) = 0$.

In practice, we have calculated explicit symbolic expressions for the functions $\xi_{\Im}^{(0)} = \xi_{\Im}^{(0)}(\eta)$, $\xi_{\Im}^{(1)} = \xi_{\Im}^{(1)}(\eta)$, and $\xi_{\Im}^{(2)} = \xi_{\Im}^{(2)}(\eta)$ using *Mathematica*; see [24] by Wolfram. (These expressions are not presented here because they are fairly cumbersome.) Then, substituting the functions $\xi_{\Im}^{(0)} = \xi_{\Im}^{(0)}(\eta)$, $\xi_{\Im}^{(1)} = \xi_{\Im}^{(1)}(\eta)$, and $\xi_{\Im}^{(2)} = \xi_{\Im}^{(2)}(\eta)$ into the second equation, $\Re Q(\xi, \eta) = 0$, we obtain the algebraic equations with respect to only one variable, η. Clearly, the above equations (which are different for the different solutions, $\xi_{\Im}^{(0)} = \xi_{\Im}^{(0)}(\eta)$, $\xi_{\Im}^{(1)} = \xi_{\Im}^{(1)}(\eta)$, $\xi_{\Im}^{(2)} = \xi_{\Im}^{(2)}(\eta)$) may have real root(s) if and only if the original equation $Q(\xi, \eta) = 0$ has other real zero(s) besides those that have already been found, $(-\omega, 0)$, $(\frac{\omega M_0}{1-M_0}, 0)$, and $(-\frac{\omega M_0}{1+M_0}, 0)$. Therefore, we have finally reduced the question about the real zeros of the equation $Q(\xi, \eta) = 0$ to the question about the real root(s) of certain algebraic equations of one variable.

Unfortunately, the resulting equations (after the substitution of $\xi_{\Im}^{(0)} = \xi_{\Im}^{(0)}(\eta)$, $\xi_{\Im}^{(1)} = \xi_{\Im}^{(1)}(\eta)$, $\xi_{\Im}^{(2)} = \xi_{\Im}^{(2)}(\eta)$ into $\Re Q(\xi, \eta) = 0$) appear too complicated for obtaining general expressions for their real root(s). However, we may implement the following seminumerical approach, which provides fairly convincing results.

First, note that the case $\omega = 0$ seems to be the simplest one. This case actually admits rigorous analysis without making any simplifying assumptions. As previously mentioned, equation (2.23) has no real solutions for ${M_0}^2 < (\frac{4}{3} + \frac{1}{\mathrm{Pr}})(\frac{7}{3} + \frac{\gamma}{\mathrm{Pr}})^{-1}$ (which implies that the determinant (2.18) has no real roots); for ${M_0}^2 = (\frac{4}{3} + \frac{1}{\mathrm{Pr}})(\frac{7}{3} + \frac{\gamma}{\mathrm{Pr}})^{-1}$, equation (2.23) degenerates; any pair (ξ, η) of the kind ξ arbitrary, $\eta = 0$, is its root. Substituting this root into $\Re Q(\xi, \eta) = 0$ (see (2.18)), we obtain $\xi^4(1/{M_0}^2 - 1) = 0$, which yields $\xi = 0$. Therefore, we have not found any new real zero. For ${M_0}^2 > (\frac{4}{3} + \frac{1}{\mathrm{Pr}})(\frac{7}{3} + \frac{\gamma}{\mathrm{Pr}})^{-1}$, equation (2.23) has two different real solutions for any η; moreover, $\xi_{\Im}^{(1)} = \xi_{\Im}^{(1)}(\eta) = -\xi_{\Im}^{(2)} = -\xi_{\Im}^{(2)}(\eta)$. Since all powers of ξ in $\Re Q(\xi, \eta)$ are even, we do not need to separately consider $\xi_{\Im}^{(1)} = \xi_{\Im}^{(1)}(\eta)$ and $\xi_{\Im}^{(2)} = \xi_{\Im}^{(2)}(\eta)$. Substituting $\xi_{\Im}^{(1,2)} = \xi_{\Im}^{(1,2)}(\eta)$ into $\Re Q(\xi, \eta) = 0$, we obtain the eighth-order equation with respect to η: $a\eta^8 + b\eta^6 + c\eta^4 = 0$, where the coefficients a, b, and c are obviously real. The explicit expressions for a, b, and c were obtained by means of *Mathematica* [24]; we do not present them here because of cumbersomeness. However, using these expressions, we can prove that $a > 0$, $b > 0$, and $c > 0$. Then, it becomes clear that there are no other real roots, except for the one we have already found, $\eta = 0$ (which also yields $\xi = 0$). Indeed, the equation $a\eta^4 + b\eta^2 + c = 0$ for $a > 0$, $b > 0$, and $c > 0$ may have only essentially complex roots η. Therefore, we conclude that for $\omega = 0$ the symbol (2.16) has only one singular point, $\xi = 0$, $\eta = 0$.

Recall that all equations under study generally depend on five real parameters, ω, M_0, Re, Pr, and γ. To simplify our task, we fix the values of some of these parameters. Namely, let us set $\gamma = 1.4$ (two-atom gas) and $\mathrm{Pr} = 0.72$ (air). This choice of values for the ratio of specific heats and for the Prandtl number, respectively, is most frequently used since it is closely related to numerous practical problems; we will not consider any other numerical values for these two parameters. We now investigate another simple case: $\omega \neq 0$, ${M_0}^2 = (\frac{4}{3} + \frac{1}{\mathrm{Pr}})(\frac{7}{3} + \frac{\gamma}{\mathrm{Pr}})^{-1}$. Then, we have

$$\xi_{\Im}^{(0)}(\eta) = -\frac{\omega}{2} + \left(\frac{\eta^2}{{M_0}^2}\left(1 + \frac{1}{\mathrm{Pr}}\right) + \frac{4}{3}\gamma\frac{\eta^4}{\mathrm{Pr}\,\mathrm{Re}^2}\right)\left(\left(\frac{7}{3} + \frac{\gamma}{\mathrm{Pr}}\right)2\omega\right)^{-1}.$$

Substituting this expression into $\Re Q(\xi, \eta)$, we obtain a 16th-order polynomial with respect to η. This polynomial contains only even degrees from 0 to 16. It is possible

to make sure (with the help of *Mathematica* [24]) that the coefficients of the above polynomial are positive $\forall\omega$, $\omega \neq 0$, and $\forall$Re; consequently, the corresponding 16th-order equation has no real roots. Therefore, the determinant (2.18) has no other real zeros in this case either.

We have finally come to the most complicated case, which so far allows us only approximate investigation. Let ${M_0}^2 < (\frac{4}{3} + \frac{1}{\mathrm{Pr}})(\frac{7}{3} + \frac{\gamma}{\mathrm{Pr}})^{-1}$. Then, we have to clarify whether the functions $\Re Q(\xi^{(1)}_{\Im}(\eta), \eta)$ and/or $\Re Q(\xi^{(2)}_{\Im}(\eta), \eta)$ turn into zero for η within the range given in the inequality (2.22). Both functions are actually of a general algebraic type (they contain noninteger powers), which means we have only a remote possibility of accurately (analytically) showing that they have no real roots, particularly because these functions depend on many parameters. At least at this point, we are unable to construct the corresponding rigorous proof, so we use the approach based on certain graphical study.

To start, we select some representative discrete set of the parameters involved. The range for the Mach number is known, so we simply choose a few points within this range. As for the Reynolds number, the representative values for the graphical analysis we will conduct may be chosen to be of the order of a few thousand. Indeed, we are not studying Stokes's flows corresponding to very low Re. As for typical laminar solutions for the flows around an airfoil, they apparently cease to exist starting from Reynolds numbers of around a few thousand. Moreover, for many practically interesting turbulent flows with true molecular Reynolds numbers of around a few million, one can successfully model turbulence in the far field by introducing a new effective value of the Reynolds number, which also appears to be of the order of a few thousand [13]. Finally, recall that the periodicity of flow in time is caused by some external influence, and [7] reports that the maximum effect of (i.e., response to) such an influence corresponds to non-dimensional frequencies of around one. Therefore, we will not consider frequencies much less than unity, or frequencies much higher than unity. Note that the upper bound for the band of frequencies originates from the numerics, since we are going to pass from the series (2.6) to the finite Fourier series while actually solving the problem on the computer (see section 3).

We also note that the limits for η (see (2.22)) do not depend on the sign of ω. Moreover, since $\xi^{(1)}_{\Im}(\eta, M_0, \mathrm{Re}, \mathrm{Pr}, \gamma, |\omega|) = -\xi^{(2)}_{\Im}(\eta, M_0, \mathrm{Re}, \mathrm{Pr}, \gamma, -|\omega|)$, $\xi^{(2)}_{\Im}(\eta, M_0, \mathrm{Re}, \mathrm{Pr}, \gamma, |\omega|) = -\xi^{(1)}_{\Im}(\eta, M_0, \mathrm{Re}, \mathrm{Pr}, \gamma, -|\omega|)$ (see (2.20)), and all powers of ξ and $(\omega + \xi)$ in $\Re Q(\xi, \eta)$ are even, it suffices to investigate the behavior of only one of the above functions for both positive and negative values of ω. We do this by plotting the corresponding graphs for the following specific values of the parameters involved: $\omega = \pm 0.5, \pm 1, \pm 10, \pm 50$; $M_0 = 0.4,\ 0.7$; $\mathrm{Re} = 1000,\ 2000,\ 5000$; γ and Pr are still 1.4 and 0.72, respectively. The graphs drawn with the help of *Mathematica* [24] in different scales show that neither of the above curves intersects the real axis. (We do not present these plots here because they are not of any interest except to show that the corresponding curve has no zeros). Relying on this approximate graphical investigation, we may expect that at least within some range of the parameters involved, the symbol (2.16) has no other real singular points, except for those that have already been found.

We use an analogous graphical approach for the case ${M_0}^2 > (\frac{4}{3} + \frac{1}{\mathrm{Pr}})(\frac{7}{3} + \frac{\gamma}{\mathrm{Pr}})^{-1}$. We have no prescribed range for η in this case. However, it is clear that the asymptotics of the functions $\Re Q(\xi^{(1,2)}_{\Im}(\eta), \eta)$ for large η is η^8, so it suffices to study the behavior of the above functions only on some finite interval of η. We used *Mathematica* [24] to plot the corresponding graphs for the same values of ω, Re, γ, Pr as

mentioned before, and for $M_0 = 0.8,\ 0.9$. The graphs (drawn in different scales for different η-intervals, up to $-10^5 < \eta < 10^5$) show that neither of the curves has real zeros in this case either.

Summarizing, we conclude that at least for a certain reasonable range of the parameters involved, M_0, Re, Pr, γ, ω, we have justified the following proposition.

PROPOSITION 2.1. *The symbol* $\mathbf{Q}(\xi, \eta)$ *(see* (2.16)*) has only three real singular points on the* (ξ, η)*-plane:* $(-\omega, 0)$, $(\frac{\omega M_0}{1-M_0}, 0)$, *and* $(-\frac{\omega M_0}{1+M_0}, 0)$. *For* $\omega = 0$, *these three points merge into one.*

To determine whether the inverse symbol $\mathbf{Q}^{-1}(\xi, \eta)$ belongs to $L^1_{loc}(R^2)$, it suffices to investigate the behavior (integrability) of this matrix function near the three singularities. This investigation actually means that we have to check integrability of each of the sixteen elements of $\mathbf{Q}^{-1}(\xi, \eta)$. These elements are given by $\left(\mathbf{Q}^{-1}\right)_{j,i} = \delta_{i,j}/Q$, $1 \le i, j \le 4$, where $\delta_{i,j}$ are the corresponding cofactors.

Let us first concentrate on the singularity $\xi = -\omega$, $\eta = 0$ for $\omega \neq 0$. We replace the above expressions for the elements of the inverse symbol by their equivalents, $\left(\mathbf{Q}^{-1}\right)_{j,i} = (\delta_{i,j}\bar{Q})/(Q\bar{Q})$ ($\bar{Q}$ means complex conjugate), to make the denominator purely real. Since both the denominator $Q\bar{Q}$ and the numerator $\delta_{i,j}\bar{Q}$ are the sums of monomials of the type $\text{const} \cdot (\omega + \xi)^k \eta^l \xi^m$ (here const depends on M_0, Re, Pr, γ, ω, and $k,\ l,\ m$ are nonnegative integers), then it is sufficient to make sure that any expression of the type

$$\frac{\left|\text{const} \cdot (\omega + \xi)^k \eta^l \xi^m\right|}{Q\bar{Q}} \tag{2.24}$$

that originates from $(\delta_{i,j}\bar{Q})/(Q\bar{Q})$, $1 \le i, j \le 4$, is integrable near $\xi = -\omega$, $\eta = 0$. Since $\omega \neq 0$, then the factors ξ^m do not contribute to the asymptotics of the expression (2.24) near $\xi = -\omega$, $\eta = 0$ (which is an essential difference in comparison with the case $\omega = 0$; see below). Therefore, we may investigate this asymptotics by constructing Newton's diagram (see [25] by Walker) with respect to only two variables, $\omega + \xi$ and η. Namely, we show in Figure 2.2 the set of points (k, l) that correspond to all monomials $\text{const} \cdot (\omega + \xi)^k \eta^l \xi^m$ involved in $Q\bar{Q}$. *The Newton diagram* [25] is a lower part of the convex hull of the above set. The diagram is shown by the dashed line in Figure 2.2. Those points (k, l) which belong to the Newton diagram are, generally speaking, those that determine the asymptotics of $Q\bar{Q}$ near $\xi = -\omega$, $\eta = 0$.

More precisely, not only is the asymptotic behavior of $Q\bar{Q}$ near the singularity determined by the lowest degree monomials (see Newton's diagram in Figure 2.2), but it may also depend on some higher-order terms if the form

$$\begin{aligned} A_Q^{(\omega)} \overset{def}{=}\ & \frac{\xi^4}{{M_0}^4}(\omega + \xi)^4 + \frac{16}{9}\frac{\xi^4}{\mathrm{Re}^4\mathrm{Pr}^2{M_0}^4}\eta^8 \\ & + \frac{\xi^4}{\mathrm{Re}^2{M_0}^4}\left[\left(\frac{4}{3} + \frac{1}{\mathrm{Pr}}\right)^2 - \frac{8}{3\mathrm{Pr}}\right](\omega + \xi)^2\eta^4 \end{aligned} \tag{2.25}$$

(which corresponds to the previously mentioned lowest-degree terms that constitute the Newton diagram) degenerates under some conditions. However, in this specific case, the form $A_Q^{(\omega)}$ of (2.25) is positive definite (because $[(\frac{4}{3} + \frac{1}{\mathrm{Pr}})^2 - \frac{8}{3\mathrm{Pr}}]$ is positive for any Pr). Therefore, after some natural change of variables (see below), the asymptotics of the denominator $Q\bar{Q}$ becomes uniform with respect to the polar angle, which implies that while investigating the integrability of $\mathbf{Q}^{-1}(\xi, \eta)$, one may simply

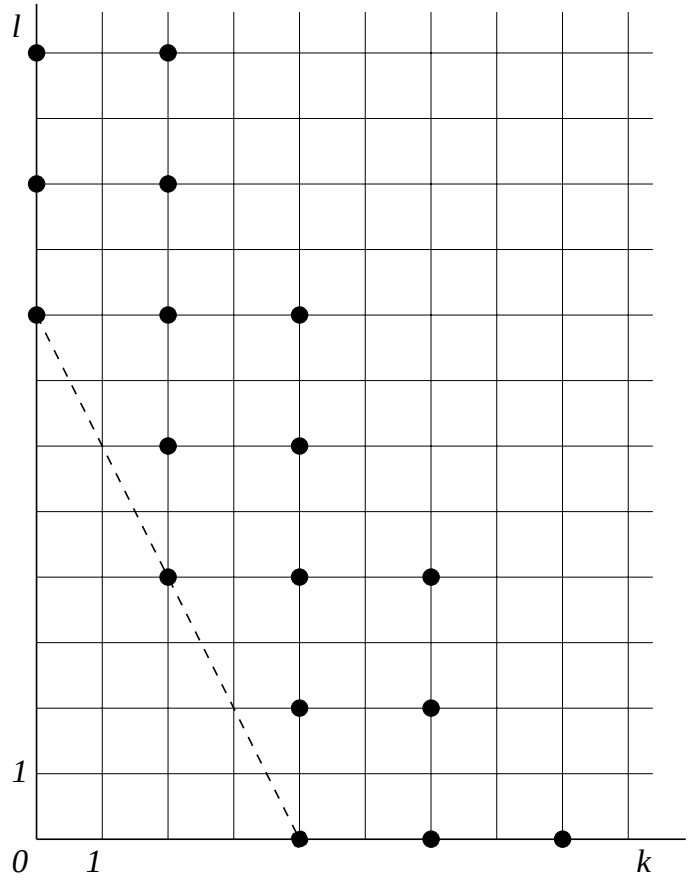

FIG. 2.2. *Powers involved in the denominator $Q\bar{Q}$ (•) and Newton's diagram for $Q\bar{Q}$; $\xi = -\omega$, $\eta = 0$ $(\omega \neq 0)$.*

neglect all higher-order terms ("bullets" above the dashed line on Figure 2.2) and consider the expression

$$\frac{\left|\text{const} \cdot (\omega+\xi)^k \eta^l \xi^m\right|}{A_Q^{(\omega)}} \tag{2.26}$$

instead of (2.24). Furthermore, we may only increase the ratio (2.26) by neglecting the third term ($\sim (\omega+\xi)^2\eta^4$) in the denominator (2.25). Indeed, it is easy to see that in doing so, we only decrease the denominator but still preserve its positive definiteness. Finally, let us eliminate the factors ξ^m, for simplicity. We have already mentioned that ξ^m do not contribute to the asymptotics of (2.26) near $\xi = -\omega$, $\eta = 0$ $(\omega \neq 0)$. Therefore, to estimate the integrals, we may replace these factors by appropriate constants, e.g.,

$$\frac{\left|\text{const} \cdot (\omega+\xi)^k \eta^l \xi^m\right|}{\frac{\xi^4}{{M_0}^4}(\omega+\xi)^4 + \frac{16}{9}\frac{\xi^4}{\text{Re}^4\text{Pr}^2{M_0}^4}\eta^8} \leq \frac{\left|\text{const} \cdot (\omega+\xi)^k \eta^l\right| |\xi|_{max}^m}{\frac{\xi_{min}^4}{{M_0}^4}(\omega+\xi)^4 + \frac{16}{9}\frac{\xi_{min}^4}{\text{Re}^4\text{Pr}^2{M_0}^4}\eta^8},$$

where minimum and maximum are found on a sufficiently small neighborhood of $\xi = -\omega$, $\eta = 0$.

Thus, we have reduced the original question of integrability of $\delta_{i,j}Q/(Q\bar{Q})$ to checking the integrability of the function

$$\frac{\left|\text{const}\cdot(\omega+\xi)^k\eta^l\right|}{a(\omega+\xi)^4+b\eta^8},\ a>0;\ b>0;\quad k,\ l\ \text{ nonnegative integers}, \tag{2.27}$$

on some neighborhood of $\xi=-\omega$, $\eta=0$. Because of the symmetry, it suffices to integrate (2.27) only on one quadrant, for example, $\omega+\xi\geq 0$, $\eta\geq 0$. Moreover, since we are studying local integrability, we also introduce some upper limits for $\omega+\xi$ and for η, e.g., $\omega+\xi\leq 1$, $\eta\leq 1$. Let us now change the variables, $\sqrt{a}(\omega+\xi)^2=\zeta$, $\sqrt{b}\eta^4=\chi$, and proceed to the following integral:

$$\text{const}\int\limits_0^1\int\limits_0^1\frac{\zeta^{(k-1)/2}\chi^{(l-3)/4}}{\zeta^2+\chi^2}d\zeta\,d\chi. \tag{2.28}$$

Further, make another change of variables, from the Cartesian $(\zeta,\ \chi)$ to polar $(\varrho,\ \theta)$ coordinates, and for simplicity, truncate our rectangular domain: $\{0\leq\zeta\leq 1,\ 0\leq\chi\leq 1\}$ $\longmapsto\ \{\zeta^2+\chi^2\leq 1\}$, which obviously does not influence the result (integrable or not integrable). Finally, instead of the integral (2.28), we obtain

$$\text{const}\int\limits_0^1\frac{\varrho^{1+(k-1)/2+(l-3)/4}}{\varrho^2}\int\limits_0^{\pi/2}(\cos\theta)^{(k-1)/2}(\sin\theta)^{(l-3)/4}d\theta\,d\varrho. \tag{2.29}$$

From (2.29) one can easily derive the conditions sufficient for the integral to exist. Namely, they are

$$\frac{k-1}{2}+\frac{l-3}{4}>\epsilon, \tag{2.30a}$$

$$\frac{k-1}{2}>\epsilon-1, \tag{2.30b}$$

$$\frac{l-3}{4}>\epsilon-1, \tag{2.30c}$$

where ϵ is an arbitrarily small positive number.

We now have to make sure that all the conditions (2.30) are satisfied for all cofactors $\delta_{i,j},\ 1\leq i,\ j\leq 4$. First, we note that since k and l are always nonnegative integers, then two conditions (2.30b) and (2.30c) are met automatically. Then, to check the fulfillment of (2.30a), one has to accurately calculate all monomials involved in all cofactors $\delta_{i,j},\ 1\leq i,\ j\leq 4$, and to analyze the powers $(k,\,l)$ for $(\omega+\xi)^k\eta^l$. This step was done with the help of *Mathematica* [24]. In Figure 2.3, we have collected all the relevant powers $(k,\,l)$ for all cofactors $\delta_{i,j},\ 1\leq i,\ j\leq 4$. We also show in Figure 2.3 the range of powers $(k,\,l)$ which satisfies conditions (2.30) (grey area). Using Figure 2.3, one can easily conclude that all monomials involved satisfy conditions (2.30); therefore, the inverse symbol $\mathbf{Q}^{-1}(\xi,\,\eta)$ is absolutely integrable near the singular point $\xi=-\omega$, $\eta=0$ $(\omega\neq 0)$.

The integrability of $\mathbf{Q}^{-1}(\xi,\,\eta)$ for $\omega=0$ near the singular point $\xi=0$, $\eta=0$ is investigated by the same method. We only note that since ξ and $\omega+\xi$ are now the same, both of them do contribute to the asymptotics of $\mathbf{Q}^{-1}(\xi,\,\eta)$ near $\xi=0$, $\eta=0$. Therefore, the sets of monomials involved, as well as the Newton diagram, for $Q\bar{Q}$ will differ noticeably from those relevant to the case $\omega\neq 0$. Indeed, the asymptotic behavior of the denominator $Q\bar{Q}$ near $\xi=0$, $\eta=0$ is now determined by the following

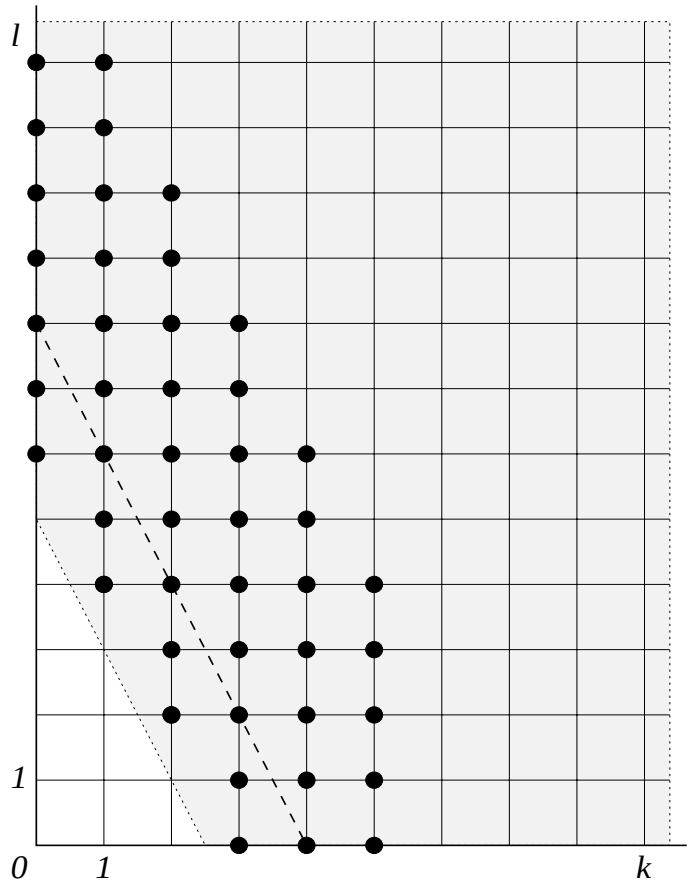

FIG. 2.3. *Powers of the monomials in cofactors* (•)*;* $\xi = -\omega$, $\eta = 0$ ($\omega \neq 0$). *Grey area corresponds to integrability conditions* (2.30).

form (compare to (2.25)):

$$A_Q^{(0)} = \left(1 + \frac{1}{{M_0}^4} - \frac{2}{{M_0}^2}\right)\xi^8 + \frac{\eta^{12}}{{M_0}^4 \mathrm{Pr}^2 \mathrm{Re}^4} + \left(\frac{2}{{M_0}^4} - \frac{2}{{M_0}^2}\right)\xi^6\eta^2 + \frac{1}{{M_0}^4}\xi^4\eta^4 + \frac{1}{{M_0}^4 \mathrm{Re}^2}\left[\left(1 + \frac{1}{\mathrm{Pr}}\right)^2 - \frac{2}{\mathrm{Pr}}\right]\xi^2\eta^8, \tag{2.31}$$

which corresponds to the Newton diagram presented in Figure 2.4.

As in the case $\omega \neq 0$, the form $A_Q^{(0)}$ (2.31) also appears positive definite, since all five coefficients in the expression (2.31) are positive $\forall$Re, Pr, $M_0 < 1$. However, the Newton diagram shown in Figure 2.4 consists of two straight intervals, whereas the one in Figure 2.2 contains only one interval. This difference is essential, because now each of the aforementioned two intervals (see the two-segment dashed polygonal line on Figure 2.4) will determine its own domain of integrability for the expressions

$$\frac{\left|\mathrm{const} \cdot \xi^k \eta^l\right|}{A_Q^{(0)}} \tag{2.32}$$

on the (k, l)-plane; here k and l are the powers in the numerator of (2.32). Since

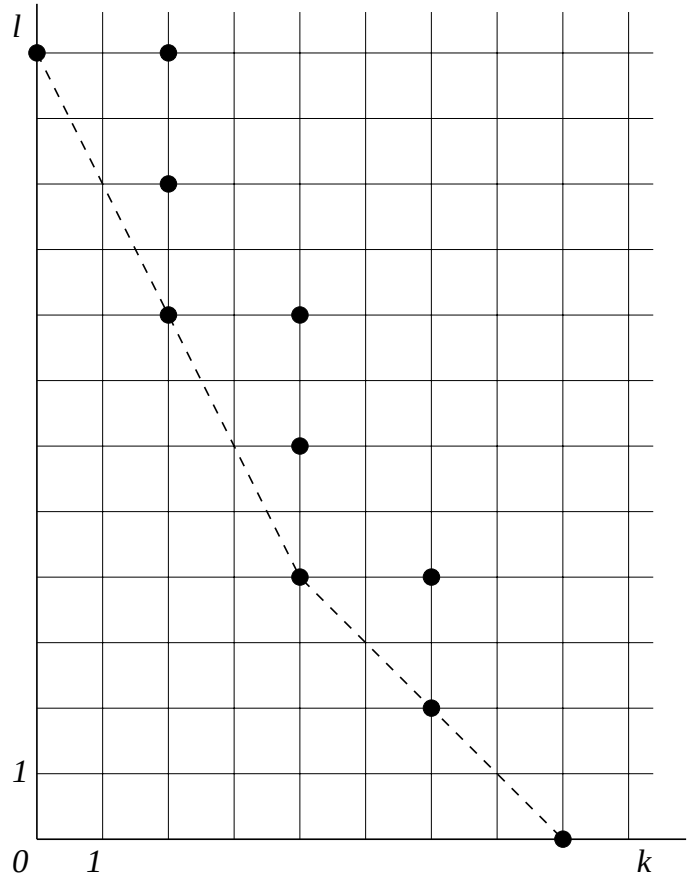

FIG. 2.4. *Powers involved in the denominator $Q\bar{Q}$ (•) and Newton's diagram for $Q\bar{Q}$; $\xi = 0$, $\eta = 0$ ($\omega = 0$).*

the form $A_Q^{(0)}$ is not simply positive definite, but all powers involved are even, and each coefficient in the expression (2.31) is positive, we can find the corresponding domain of integrability on the (k, l)-plane independently for each of the two parts of the Newton diagram; see Figure 2.4.

To do this for either part of the diagram, we neglect those terms in the denominator which correspond to another part (in so doing, the denominator may only decrease). Then, we formally divide both the numerator and the denominator by the common factor ξ^4 and, using the changes of variables analogous to those implemented above, come to the following set of conditions sufficient for the integrability of the function (2.32) near $\xi = 0$, $\eta = 0$:

$$\frac{k-1}{2} + \frac{l-7}{4} > \epsilon, \tag{2.33a}$$

$$\frac{k-1}{2} > \epsilon - 1, \tag{2.33b}$$

$$\frac{l-7}{4} > \epsilon - 1, \tag{2.33c}$$

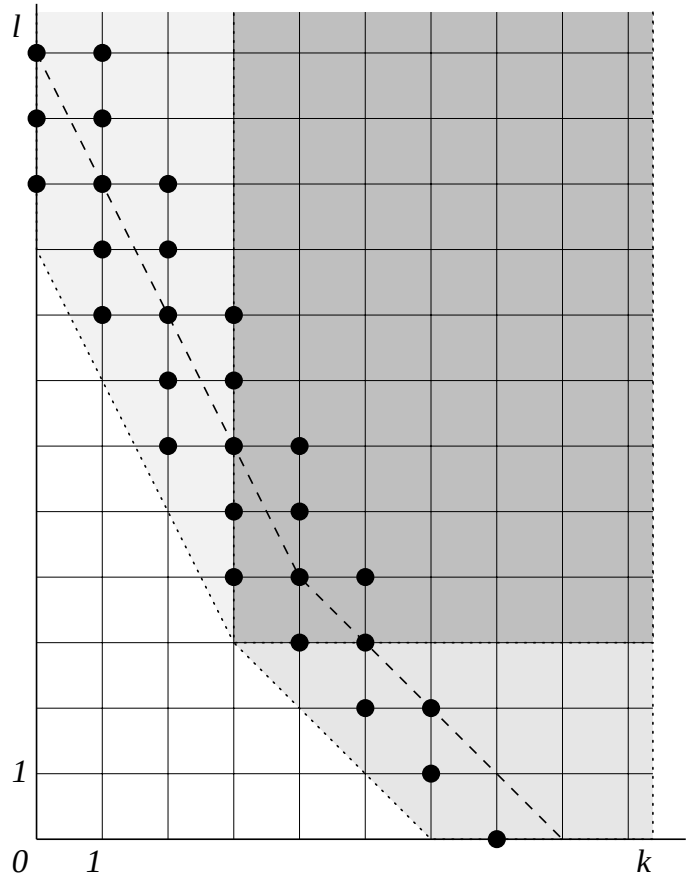

FIG. 2.5. *Powers of the monomials in cofactors* (•)*;* $\xi = 0$, $\eta = 0$ ($\omega = 0$). *Light-grey area corresponds to integrability conditions* (2.33)*; middle-grey area corresponds to integrability conditions* (2.34)*; dark-grey area is common to both* (2.33) *and* (2.34).

and

$$\frac{k-5}{2} + \frac{l-1}{2} > \epsilon, \tag{2.34a}$$

$$\frac{k-5}{2} > \epsilon - 1, \tag{2.34b}$$

$$\frac{l-1}{2} > \epsilon - 1. \tag{2.34c}$$

Note that the three conditions (2.33) correspond to the upper part of the Newton diagram, and conditions of (2.34) correspond to its lower part (see Figure 2.4).

In Figure 2.5, we show (by "bullets") all powers (k, l) involved in all cofactors $\delta_{i,j},\ 1 \le i,\ j \le 4$, for the case $\omega = 0$. Grey areas on this figure correspond to the range of the coefficients (k, l) that satisfy the integrability conditions (2.33), (2.34). Note that the conditions (2.33c) and (2.34b) impose some additional restrictions on l and k for the upper and lower components, respectively, of the Newton diagram in Figure 2.5. We do not have such restrictions in the case $\omega \neq 0$; see (2.30). One can

easily see from Figure 2.5 that all elements of $\mathbf{Q}^{-1}$, $(\delta_{i,j}\bar{Q})/(Q\bar{Q})$, $1 \le i,\ j \le 4$, are absolutely integrable near $\xi = 0$, $\eta = 0$ in the case $\omega = 0$ as well.

Finally, we only have to show that $\mathbf{Q}^{-1}(\xi,\,\eta)$ is absolutely integrable on some neighborhood of each of the singular points $(\frac{\omega M_0}{1-M_0},\,0)$ and $(-\frac{\omega M_0}{1+M_0},\,0)$ for $\omega \neq 0$. Clearly, if we simply ensure that $\left|Q^{-1}(\xi,\,\eta)\right|$ is integrable on the same neighborhood, then the integrability of $\mathbf{Q}^{-1}(\xi,\,\eta)$ follows. To do this, first note that $\operatorname{grad} Q(\xi,\,\eta) \neq \mathbf{0}$ at either of these two points. Indeed, it is easy to see from (2.18) that $\frac{\partial Q}{\partial \xi} \neq 0$ at both $(\frac{\omega M_0}{1-M_0},\,0)$ and $(-\frac{\omega M_0}{1+M_0},\,0)$ $\forall M_0 < 1$. Then, refer to work by Vainberg [26], where the author proves exactly the same statement we need, namely, the integrability of $\left|Q^{-1}(\xi,\,\eta)\right|$ on some neighborhood of an isolated real zero of the polynomial $Q(\xi,\,\eta)$ when $\operatorname{grad} Q(\xi,\,\eta) \neq \mathbf{0}$ at this point.

Thus, we can finally formulate the following proposition.

PROPOSITION 2.2. *The inverse symbol* $\mathbf{Q}^{-1}(\xi,\,\eta)$ *(see* (2.16)*) is absolutely integrable on any finite domain of* R^2*; i.e.,* $\mathbf{Q}^{-1}(\xi,\,\eta) \in L^1_{loc}(R^2)$.

In accordance with [23], Proposition 2.2 immediately implies the existence.

PROPOSITION 2.3 (existence). *For any compactly supported* $\hat{\mathbf{f}} \in L^1(R^2)$*, the system* (2.15) *with* $\hat{\hat{\mathbf{f}}}$ *defined by formula* (2.14b) *is solvable in* $\mathcal{G}'$.

The solution to the AP (2.12)–(2.13) that we are looking for can now be found by means of the inverse Fourier transform (again, the superscript n is omitted below):

$$\hat{\mathbf{u}}(x,\,y) = \frac{1}{2\pi}\int\limits_{-\infty}^{\infty}\int\limits_{-\infty}^{\infty} \hat{\hat{\mathbf{u}}}(\xi,\,\eta)\, e^{i\xi x + i\eta y} d\xi\, d\eta. \tag{2.35}$$

Using the brief notation, we may rewrite (2.35) as $\hat{\mathbf{u}} = (\hat{\hat{\mathbf{u}}})^{\check{}} = (\mathbf{Q}^{-1}\hat{\hat{\mathbf{f}}})^{\check{}}$. However, in so doing we still do not know whether the function $\hat{\mathbf{u}}(x,\,y)$ of (2.35) satisfies the boundary condition (2.13). Let us first prove the following proposition.

PROPOSITION 2.4 (uniqueness). *If the solution* $\hat{\mathbf{u}}$ *of the system* (2.12) *satisfies boundary condition* (2.13)*, then it is unique in the class of distributions vanishing at infinity.*

Proof. Any function $\hat{\mathbf{u}}$ that solves (2.12) is actually an inverse Fourier transform of some solution to the system (2.15), $\hat{\mathbf{u}} = (\hat{\hat{\mathbf{u}}})^{\check{}}$. In turn, any distribution $\hat{\hat{\mathbf{u}}} \in \mathcal{G}'$ that solves (2.15) (see (2.17)) should coincide with the regular function $\mathbf{Q}^{-1}(\xi,\,\eta)\hat{\hat{\mathbf{f}}}(\xi,\,\eta)$ everywhere on R^2, except at the three singular points of $\mathbf{Q}(\xi,\,\eta)$ (since $\hat{\hat{\mathbf{f}}}(\xi,\,\eta)$ has no singular points). Therefore, any other solution to (2.15) may differ from $\hat{\hat{\mathbf{u}}}$ only by a distribution with the support belonging to the three-point set

$$\left\{(-\omega,\,0),\ \left(\frac{\omega M_0}{1-M_0},\,0\right),\ \left(-\frac{\omega M_0}{1+M_0},\,0\right)\right\}.$$

Such a distribution may only be a finite sum of δ-functions and their derivatives [23]. Therefore, if $\hat{\mathbf{u}} = (\hat{\hat{\mathbf{u}}})^{\check{}}$ vanishes at infinity, then any other solution to (2.12) will differ from $\hat{\mathbf{u}}$ by an inverse Fourier transform of a finite sum of δ-functions and their derivatives, and, consequently, it will not vanish at infinity since Fourier transforms of δ-functions and their derivatives are polynomials [23]. Thus, Proposition 2.4 is justified. ∎

Let us now select a finite ball B, $B \subset R^2$. By $B-\epsilon$ and $B+\epsilon$ we denote the balls with the radii $r_B - \epsilon$ and $r_B + \epsilon$, respectively, where r_B is the radius of B ($\epsilon > 0$). We require that

$$B - \epsilon \supset \left\{(-\omega,\, 0),\ \left(\frac{\omega M_0}{1-M_0},\, 0\right),\ \left(-\frac{\omega M_0}{1+M_0},\, 0\right)\right\}$$

and construct a partition of unity, $1 = g_B + g_{\bar{B}}$, where the functions g_B and $g_{\bar{B}}$ are infinitely smooth and bounded on R^2. By definition, the function g_B is identically zero outside the ball $B+\epsilon$; therefore, $g_{\bar{B}}$ is identically zero inside the ball $B-\epsilon$. Note that such functions always exist (see, e.g., [23]). Obviously, $\hat{\mathbf{u}} = (\mathbf{Q}^{-1}\hat{\hat{\mathbf{f}}})^{\check{}} = (\mathbf{Q}^{-1}g_B\hat{\hat{\mathbf{f}}})^{\check{}} + (\mathbf{Q}^{-1}g_{\bar{B}}\hat{\hat{\mathbf{f}}})^{\check{}}$. We will separately analyze each term on the right-hand side of the above sum. First, it is clear that $\mathbf{Q}^{-1}g_B\hat{\hat{\mathbf{f}}} \in L^1(R^2)$ because $\hat{\hat{\mathbf{f}}}$ is bounded and $\mathbf{Q}^{-1} \in L^1_{loc}(R^2)$. Therefore, $(\mathbf{Q}^{-1}g_B\hat{\hat{\mathbf{f}}})^{\check{}} \longrightarrow 0$ while $\sqrt{x^2+y^2} \longrightarrow \infty$. For the second term $(\mathbf{Q}^{-1}g_{\bar{B}}\hat{\hat{\mathbf{f}}})^{\check{}}$, we cannot yet construct a general proof of its decay at infinity. The difficulties here arise from the fact that $\mathbf{Q}^{-1} \in L^1_{loc}(R^2)$ but $\mathbf{Q}^{-1} \notin L^1(R^2)$; i.e., it is not absolutely integrable near infinity. Therefore, a general proof may require an appropriate regularization of the corresponding oscillatory integral. However, we retain this question for a future investigation. For the time being, we can formulate the following two statements. Each will address the vanishing of the solution at infinity for some particular case (or in a weaker formulation).

First, assume that $\hat{\mathbf{f}} \in L^2(R^2)$, which is actually not restrictive for our purposes. Then, $\hat{\hat{\mathbf{f}}} \in L^2(R^2)$ (we may treat the Fourier transform here in the sense of Plancherel). As mentioned before, $\mathbf{Q}^{-1} \notin L^1(R^2)$; however, $\mathbf{Q}^{-1}g_{\bar{B}}$ can be shown to be bounded on R^2. Therefore, $\mathbf{Q}^{-1}g_{\bar{B}}\hat{\hat{\mathbf{f}}} \in L^2(R^2)$, which immediately yields $(\mathbf{Q}^{-1}g_{\bar{B}}\hat{\hat{\mathbf{f}}})^{\check{}} \in L^2(R^2)$. Thus, in this case the solution $\hat{\mathbf{u}}$ to the system (2.12) is represented as a sum of two terms, $\hat{\mathbf{u}}^{(1)} + \hat{\mathbf{u}}^{(2)}$, where $\hat{\mathbf{u}}^{(1)} \longrightarrow 0$ while $\sqrt{x^2+y^2} \longrightarrow \infty$ (true vanishing in the sense of (2.13)) and $\hat{\mathbf{u}}^{(2)} \in L^2(R^2)$, which may be treated as a "generalized decay." We also note here that the statement on uniqueness proven in Proposition 2.4 also applies to the functions from $L^2(R^2)$, since the polynomials obviously do not belong to $L^2(R^2)$.

Second, if we impose some additional restrictions on $\hat{\mathbf{f}}$, namely, if we require that $\hat{\mathbf{f}}$ be sufficiently smooth on R^2 so that $\hat{\hat{\mathbf{f}}} \in L^1(R^2)$, then we obtain a true decay for the second term as well, $(\mathbf{Q}^{-1}g_{\bar{B}}\hat{\hat{\mathbf{f}}})^{\check{}} \longrightarrow 0$ while $\sqrt{x^2+y^2} \longrightarrow \infty$. Therefore, for a more particular class of the right-hand sides, we may affirm that the problem (2.12)–(2.13) is uniquely solvable in $\mathcal{G}'$. We note that for many different cases (see [9]) such a restriction of the class of admissible right-hand sides does not influence the construction of the DPM-based numerical algorithm.

2.3. Truncation of the linearized problem. As mentioned in section 2.1, the domain D_{ex} must be truncated in order to numerically solve (2.8)–(2.9)–(2.10). In the framework of DPM, it suffices to construct an equivalent finite substitute for the auxiliary problem (2.12)–(2.13). Below, this is done after introducing some simplifying assumptions in regard to both the smoothness of the solution we are looking for as well as the rate of its decay at infinity. This enables us to avoid unnecessary complications that are not essential for the purpose of constructing the numerical algorithm.

For reasons of numerical convenience and effectiveness, we will use a different method for solving the AP, rather than the one from section 2.2. Using this new solution technique, we will equivalently reformulate the AP on a new finite domain. Namely, let us again take the Fourier transform of both sides of the system (2.12); however, now we do so only in one Cartesian direction, y (compare to (2.14)):

$$\hat{\hat{\mathbf{u}}}(x,\,\eta) = \frac{1}{\sqrt{2\pi}} \int\limits_{-\infty}^{\infty} \hat{\mathbf{u}}(x,\,y)\, e^{-i\eta y}\, dy, \tag{2.36a}$$

$$\hat{\hat{\mathbf{f}}}(x,\,\eta) = \frac{1}{\sqrt{2\pi}} \int\limits_{-\infty}^{\infty} \hat{\mathbf{f}}(x,\,y)\, e^{-i\eta y}\, dy. \tag{2.36b}$$

(Again, we drop the subscript n hereafter in this subsection to simplify the notations. Moreover, we retain here the same notations, $\hat{\mathbf{u}}$ and $\hat{\hat{\mathbf{f}}}$, as in section 2.2; however, the left-hand sides of the expressions (2.14) and (2.36) are obviously not the same.) Then, we obtain the following family of systems of ordinary differential equations (ODEs):

$$\frac{d\hat{\hat{\mathbf{u}}}(x,\,\eta)}{d\,x} + \mathbf{Q}(\eta)\hat{\hat{\mathbf{u}}}(x,\,\eta) = \tilde{\mathbf{f}}(x,\,\eta), \tag{2.37}$$

where

$$\mathbf{Q}(\eta) = \mathbf{D}^{-1} \begin{bmatrix} 0 & i\eta & 0 & i\omega \\ i\omega + \frac{\eta^2}{\mathrm{Re}} & 0 & 0 & 0 \\ 0 & i\omega + \frac{4}{3}\frac{\eta^2}{\mathrm{Re}} & i\eta & 0 \\ 0 & 0 & i\omega + \frac{\gamma\eta^2}{\mathrm{Re\,Pr}} & -\frac{i\omega}{{M_0}^2} - \frac{\eta^2}{\mathrm{Re\,Pr}\,{M_0}^2} \end{bmatrix} \tag{2.38a}$$

and

$$\tilde{\mathbf{f}}(x,\,\eta) = \mathbf{D}^{-1}\hat{\hat{\mathbf{f}}}(x,\,\eta). \tag{2.38b}$$

The matrix $\mathbf{D}$ from (2.38) is defined in (2.3b). Note that $\mathbf{Q}$ from (2.38a) and $\mathbf{Q}$ from (2.16) are not the same. The family (2.37) is parameterized by the continuous variable η, $-\infty < \eta < \infty$, and x in (2.37) is an independent variable. Recall that the solution $\hat{\mathbf{u}}(x,\,y)$ we are going to calculate should vanish at infinity (see (2.13)). Consequently, we will generally impose the following boundary condition on the solution of (2.37):

$$\hat{\hat{\mathbf{u}}}(x,\,\eta) \longrightarrow 0, \quad \text{as } |x| \longrightarrow \infty. \tag{2.39a}$$

However, in particular cases (see below and [8] for details) the condition (2.39a) may appear too restrictive, namely, the cases when $\mathbf{Q}(\eta)$ has purely imaginary (or zero) eigenvalues. Therefore, for some selected values of ω and η, we will only require

$$\left|\hat{\hat{\mathbf{u}}}(x,\,\eta)\right| \le \text{const}, \quad \text{as } |x| \longrightarrow \infty. \tag{2.39b}$$

Note that we do not consider solutions that grow polynomially; the latter solutions correspond to the case when $\mathbf{Q}(\eta)$ has multiple purely imaginary eigenvalues and does not have a basis composed of eigenvectors.

Once we are able to find (for all η) a solution to the system (2.37) that would satisfy boundary conditions (2.39) at infinity, then the solution to the AP (2.12)–(2.13) can be restored by means of a one-dimensional inverse Fourier transform:

$$\hat{\mathbf{u}}(x,\, y) = \frac{1}{\sqrt{2\pi}} \int\limits_{-\infty}^{\infty} \hat{\hat{\mathbf{u}}}(x,\, \eta)\, e^{i\eta y}\, d\eta. \tag{2.40}$$

Let us designate the inverse operator for the one-dimensional problem (2.37)–(2.39) by $\mathbf{G}_x(\eta)$. That is, the solution $\hat{\hat{\mathbf{u}}}(x,\, \eta)$ to this problem is given by

$$\hat{\hat{\mathbf{u}}}(x,\, \eta) = \mathbf{G}_x(\eta)\hat{\hat{\mathbf{f}}}(x,\, \eta). \tag{2.41}$$

The operator $\mathbf{G}_x(\eta)$ is obviously linear. Combining the formulas (2.36), (2.40), and (2.41), we obtain the following formula for the solution of the AP (2.12)–(2.13):

$$\hat{\mathbf{u}}(x,\, y) = \frac{1}{2\pi} \int\limits_{-\infty}^{\infty} \mathbf{G}_x(\eta) \int\limits_{-\infty}^{\infty} \hat{\mathbf{f}}(x,\, s) e^{-i(s-y)\eta} ds\, d\eta. \tag{2.42a}$$

Now, we will show how one can pass from the AP (2.12)–(2.13) to the new AP formulated on the strip $\{-\infty < x < \infty\} \times \{-\frac{Y}{2} \le y \le \frac{Y}{2}\}$ and periodic in the y direction, Y being the value of the period. In doing so, we expect that when the period Y grows, $Y \longrightarrow +\infty$, the solution to the new periodic AP will uniformly converge to the solution of the original AP (2.12)–(2.13) on any strip $\{-\infty < x < \infty\} \times \{-\breve{y} \le y \le \breve{y}\}$ where $\breve{y}$ *is fixed* and always less than $\frac{Y}{2}$. Note that the same approach was used in [8] for the steady-state problems.

Hereafter, we assume that all functions involved are defined on the infinite strip $\{-\infty < x < \infty\} \times \{-\frac{Y}{2} \le y \le \frac{Y}{2}\}$. The width of the strip Y is initially supposed to be greater than the diameter of $\operatorname{supp}\hat{\mathbf{f}}$ (later, we will consider the limit $Y \longrightarrow +\infty$). We assume periodicity of the solution to the new AP in the y direction. Then, the solution that vanishes as $|x| \longrightarrow \infty$ is given by

$$\hat{\mathbf{u}}_Y(x,\, y) = \sum_{k=-\infty}^{k=\infty} \mathbf{G}_x\left(\frac{2\pi k}{Y}\right) \frac{1}{Y} \int\limits_{-Y/2}^{Y/2} \hat{\mathbf{f}}(x,\, s) e^{-i\frac{2\pi k}{Y}(s-y)} ds. \tag{2.42b}$$

In formula (2.42b), we used the Fourier series of a periodic function instead of the Fourier integral used in the formula (2.42a). Our goal is to estimate $|\hat{\mathbf{u}}(x,\, y) - \hat{\mathbf{u}}_Y(x,\, y)|$ from above on a finite (fixed) interval $(-\breve{y}, \breve{y})$, $\breve{y} < \frac{Y}{2}$, uniformly with respect to x. Let us introduce a uniform mesh in η, where $h_\eta = 2\pi/Y$ is the mesh size, and designate $\eta_k = k\, h_\eta$, $k = 0, \pm 1, \pm 2, \ldots$. Let us then fix some interval $(-\mathcal{A}, \mathcal{A})$; we will always choose h_η (and consequently, Y) so that $\mathcal{A} = h_\eta(K + 1/2)$, K being integer. Then,

$$|\hat{\mathbf{u}}(x,\, y) - \hat{\mathbf{u}}_Y(x,\, y)|$$

$$= \frac{1}{2\pi} \left| \int\limits_{-\infty}^{\infty} \mathbf{G}_x(\eta) \int\limits_{-\infty}^{\infty} \hat{\mathbf{f}}(x,\, s) e^{-i(s-y)\eta} ds\, d\eta - \sum_{k=-\infty}^{k=\infty} h_\eta \mathbf{G}_x(\eta_k) \int\limits_{-Y/2}^{Y/2} \hat{\mathbf{f}}(x,\, s) e^{-i\eta_k(s-y)} ds \right|$$

$$\le \frac{1}{2\pi} \left| \int\limits_{-\mathcal{A}}^{\mathcal{A}} \ldots - \sum_{k=-K}^{k=K} \ldots \right| + \frac{1}{2\pi} \left| \int\limits_{|\eta|>\mathcal{A}} \ldots - \sum_{|k|>K} \ldots \right| = \frac{1}{2\pi} |\cdot|_1 + \frac{1}{2\pi} |\cdot|_2.$$

Let us separately estimate each of the two terms above (the first one corresponds to the finite interval, and the second one corresponds to the complementary infinite interval).

$$\begin{aligned}
&\frac{1}{2\pi}\,|\cdot|_1 \\
&\le \frac{1}{2\pi}\sum_{k=-K}^{k=K}\left|\int_{(K-1/2)h_\eta}^{(K+1/2)h_\eta}\mathbf{G}_x(\eta)\int_{-\infty}^{\infty}\hat{\mathbf{f}}(x,\,s)e^{-i(s-y)\eta}ds\,d\eta\right. \\
&\qquad\left. -\,h_\eta\mathbf{G}_x(\eta_k)\int_{-Y/2}^{Y/2}\hat{\mathbf{f}}(x,\,s)e^{-i\eta_k(s-y)}ds\right| \\
&\le \frac{1}{2\pi}\sum_{k=-K}^{k=K}\left(\left|\int_{(K-1/2)h_\eta}^{(K+1/2)h_\eta}\mathbf{G}_x(\eta)\int_{-\infty}^{\infty}\hat{\mathbf{f}}(x,\,s)e^{-i(s-y)\eta}ds\,d\eta\right.\right. \\
&\qquad\left. -h_\eta\mathbf{G}_x(\eta_k)\int_{-\infty}^{\infty}\hat{\mathbf{f}}(x,\,s)e^{-i\eta_k(s-y)}ds\right| \\
&\qquad\left. +\,h_\eta\left|\mathbf{G}_x(\eta_k)\int_{|s|>Y/2}\hat{\mathbf{f}}(x,\,s)e^{-i\eta_k(s-y)}ds\right|\right)
\end{aligned}$$

Clearly, the right-hand side of the previous inequality is actually the sum of errors of the quadrature formula of rectangles for the function

$$\hat{\hat{\mathbf{u}}}(x,\,\eta)e^{i\eta y}=\mathbf{G}_x(\eta)\int_{-\infty}^{\infty}\hat{\mathbf{f}}(x,\,s)e^{-i\eta(s-y)}ds$$

(see (2.41)) on elementary segments of the kind $[(k-1/2)h_\eta,\,(k+1/2)h_\eta]$, $k=-K,\ldots,K$. Indeed, for each k, $k=-K,\ldots,K$, the third term that corresponds to the integration over $|s|>\frac{Y}{2}$ turns into zero for sufficiently large Y's since $\hat{\mathbf{f}}(x,\,s)$ is compactly supported. Therefore, one can obtain the following estimate:

$$\begin{aligned}
&\frac{1}{2\pi}\,|\cdot|_1 \le \text{const}\cdot {h_\eta}^2\mathcal{A}\max_{\substack{x\in R\\ \eta\in(-\mathcal{A},\,\mathcal{A})}}\left|\frac{\partial^2}{\partial\eta^2}\left(\hat{\hat{\mathbf{u}}}(x,\,\eta)e^{i\eta y}\right)\right| \\
&\le \text{const}\cdot {h_\eta}^2\mathcal{A}\max_{\substack{x\in R\\ \eta\in(-\mathcal{A},\,\mathcal{A})}}\left(\left|\frac{\partial^2\hat{\hat{\mathbf{u}}}(x,\,\eta)}{\partial\eta^2}\right|+2|y|\left|\frac{\partial\hat{\hat{\mathbf{u}}}(x,\,\eta)}{\partial\eta}\right|+y^2\left|\hat{\hat{\mathbf{u}}}(x,\,\eta)\right|\right) \\
&=\left(c_1+c_2|y|+c_3y^2\right){h_\eta}^2\mathcal{A},\quad c_1,\,c_2,\,c_3>0.
\end{aligned}$$

Note that if we initially assume that the solution $\hat{\mathbf{u}}(x,\,y)$ decreases at infinity sufficiently fast, then the differentiability of its Fourier transform $\hat{\hat{\mathbf{u}}}(x,\,\eta)$ (see the right-hand side of the above inequality) follows directly.

For the second expression, we obtain

$$\frac{1}{2\pi}\,|\cdot|_2 \le \frac{1}{2\pi}\left(\int\limits_{|\eta|>\mathcal{A}}\left|\mathbf{G}_x(\eta)\int\limits_{-\infty}^{\infty}\hat{\mathbf{f}}(x,\,s)e^{-i\eta(s-y)}ds\right|d\eta + \sum_{|k|>K} h_\eta\left|\mathbf{G}_x(\eta_k)\int\limits_{-Y/2}^{Y/2}\hat{\mathbf{f}}(x,\,s)e^{-i\eta_k(s-y)}ds\right|\right).$$

Let us replace the integration limits $\int_{-Y/2}^{Y/2}$ in the second term on the right-hand side of this inequality by $\int_{-\infty}^{\infty}$, as was done while estimating $|\cdot|_1$. Then,

$$\frac{1}{2\pi}\,|\cdot|_2 \le \frac{1}{2\pi}\left(\int\limits_{|\eta|>\mathcal{A}}\left|\hat{\mathbf{u}}(x,\,\eta)\right|d\eta + \sum_{|k|>K} h_\eta\left|\hat{\mathbf{u}}(x,\,\eta_k)\right|\right).$$

Additionally, let us assume that the solution we are looking for has two absolutely integrable derivatives. Then its Fourier transform decreases faster than $|\eta|^{-2}$, and the previous inequality directly implies

$$\frac{1}{2\pi}\,|\cdot|_2 \le \frac{c_4}{\mathcal{A}},\quad c_4>0.$$

Combining the two obtained estimates, one easily gets

$$|\hat{\mathbf{u}}(x,\,y)-\hat{\mathbf{u}}_Y(x,\,y)| \le c_0 {h_\eta}^2\mathcal{A}+\frac{c_4}{\mathcal{A}},$$

where $c_0 \overset{def}{=} \max_{y\in(-\breve{y},\,\breve{y})}(c_1+c_2|y|+c_3y^2)$, $c_0>0$. Clearly, all constants involved in the foregoing estimates depend, generally speaking, on the specific nonperiodic function $\hat{\mathbf{u}}(x,\,y)$ that we approximate by the periodic functions $\hat{\mathbf{u}}_Y(x,\,y)$.

Now let ϵ be an arbitrary positive number. We will choose sufficiently large Y_ϵ (i.e., sufficiently small h_{η_ϵ}) so that the inequality

$$c_0 {h_\eta}^2\mathcal{A}+\frac{c_4}{\mathcal{A}}<\epsilon \tag{2.43}$$

is satisfied $\forall Y > Y_\epsilon$. In other words, we require that for a prescribed ϵ and for any $h_\eta < h_{\eta_\epsilon}$, the inequality (2.43) has real positive solutions $\mathcal{A}$ of the special kind $\mathcal{A}=(K+1/2)h_\eta$ (K being integer). The latter requirement is always met once, e.g., the distance between the real roots of the quadratic equation $c_0 {h_\eta}^2\mathcal{A}^2-\epsilon\mathcal{A}+c_4=0$ is greater than h_η. This, in turn, yields the inequality $\epsilon^2-4c_0c_4{h_\eta}^2-{c_0}^2{h_\eta}^6>0$ for h_η. This inequality is obviously satisfied for any $0\le h_\eta<h_{\eta_\epsilon}$, where $h_{\eta_\epsilon}\in R$ is a unique positive root of the equation $\epsilon^2-4c_0c_4{h_\eta}^2-{c_0}^2{h_\eta}^6=0$. Since the fulfillment of the inequality (2.43) is sufficient for the estimate

$$|\hat{\mathbf{u}}(x,\,y)-\hat{\mathbf{u}}_Y(x,\,y)|<\epsilon \tag{2.44}$$

to be true, then we have shown that $\forall\epsilon>0$, one can always find a sufficiently large period Y_ϵ so that for any $Y>Y_\epsilon$, the absolute value of the discrepancy

between the nonperiodic solution $\hat{\mathbf{u}}(x, y)$ and its periodic approximation $\hat{\mathbf{u}}_Y(x, y)$, $|\hat{\mathbf{u}}(x, y) - \hat{\mathbf{u}}_Y(x, y)|$, does not exceed ϵ for all x and for all $-\breve{y} \le y \le \breve{y}$.

Thus, we have reduced the original AP (2.12)–(2.13) to the new AP formulated on the strip $\{-\infty < x < \infty\} \times \{-\frac{Y}{2} \le y \le \frac{Y}{2}\}$. In section 3, we show that we will only need to know the solution of the AP in some neighborhood of $\mathrm{supp}\hat{\mathbf{f}}$; therefore, the approximation of the nonperiodic function $\hat{\mathbf{u}}(x, y)$ by a periodic one, $\hat{\mathbf{u}}_Y(x, y)$, *only on a finite interval* $-\breve{y} \le y \le \breve{y}$ is sufficient for our purposes. Let us now show how to pass from the domain $\{-\infty < x < \infty\} \times \{-\frac{Y}{2} \le y \le \frac{Y}{2}\}$, which is still infinite, to a truly finite domain for the new AP.

Instead of $\{-\infty < x < \infty\} \times \{-\frac{Y}{2} \le y \le \frac{Y}{2}\}$, let us now consider a rectangular domain $D_Y^0 = (0, X) \times (-Y/2, Y/2)$ (see Figure 2.1). This new domain D_Y^0 should completely contain Γ and Γ_1. We will reformulate the new AP so that its solution will be determined only on this finite domain D_Y^0 and will coincide there with the corresponding fragment of the solution found on $\{-\infty < x < \infty\} \times \{-\frac{Y}{2} \le y \le \frac{Y}{2}\}$ before the reformulation. As previously mentioned, we only need to calculate the solution to the AP in some neighborhood of D_{in}. Therefore, we are always able to choose an appropriate X and Y so that this neighborhood belongs to D_Y^0, and consequently, we only need to construct special boundary conditions at the lines $x = 0$ and $x = X$, so that the reformulated new AP being solved on D_Y^0 is equivalent to the periodic AP on the strip $\{-\infty < x < \infty\} \times \{-\frac{Y}{2} \le y \le \frac{Y}{2}\}$ described above. These boundary conditions at $x = 0$ and $x = X$ will be set separately for each wavenumber k, $k = 0, \pm 1, \pm 2, \ldots$ (see (2.42b)) involved in the Fourier representation of the function $\hat{\mathbf{u}}_Y(x, y)$. Namely, for each k, $k = 0, \pm 1, \pm 2, \ldots$, we require that the corresponding Fourier mode $\hat{\hat{\mathbf{u}}}(x, \eta_k) \equiv \hat{\hat{\mathbf{u}}}(x, 2\pi k/Y)$ meets the boundary conditions (2.39) at infinity. To exactly transfer the boundary conditions (2.39) from infinity to the finite boundaries $x = 0$ and $x = X$, we use the following consideration. Since (2.37) is the system of ODEs with constant coefficients, and since it is homogeneous outside $(0, X)$ (recall that $\mathrm{supp}\hat{\mathbf{f}}(x, y) \subset D_{in}$, and consequently, $\mathrm{supp}\hat{\hat{\mathbf{f}}}(x, \eta) \subset (0, X)\ \forall \eta$), then it obviously has four linearly independent eigensolutions (in the region of homogeneity). Depending on the structure of the set of eigenvalues of the matrix $\mathbf{Q}(\eta)$, these eigensolutions may either increase or decrease exponentially or oscillate as $x \longrightarrow +\infty$ and as $x \longrightarrow -\infty$. The case of decrease corresponds to the boundary conditions (2.39a); the oscillatory case corresponds to the boundary conditions (2.39b). As previously mentioned, we do not consider the last possible case when $\mathbf{Q}(\eta)$ has multiple purely imaginary (or zero) eigenvalues and does not have a basis composed of eigenvectors, which leads to polynomially growing solutions. Sometimes one can analytically make sure that this case really does not take place. For example, we do so in section 3 in the discrete formulation for some particular values of ω and η. In other situations, this question may require some additional numerical investigation as in [8]. At any rate, to satisfy the boundary conditions (2.39), we must prohibit at $x = 0$ all solutions that do not decrease to the left (i.e., as $x \longrightarrow -\infty$), and prohibit at $x = X$ all solutions that increase to the right (i.e., as $x \longrightarrow +\infty$). The reason for this asymmetry was mentioned before: once we have purely imaginary (or zero) eigenvalues of $\mathbf{Q}(\eta)$ and, consequently, oscillating or constant-in-space solutions (see (2.39b)), then we cannot always prohibit at both ends of the interval $(0, X)$ all modes that do not decrease in the corresponding direction. However, it should not affect the result, since the final solution we are looking for, $\hat{\mathbf{u}}(x, y)$, decreases at infinity (see section 2.2). Moreover, we have proven in [8]

that once we have a selected nondecreasing mode in Fourier representation of the solution, then after the inverse Fourier transform, the entire solution will nevertheless decrease. Therefore, we can take into account selected nondecreasing modes (if any) by simply admitting them at one of the two boundaries, $x = 0$ or $x = X$. (If we do not do this, the problem may appear overdetermined.) It seems more natural to admit the nondecreasing Fourier modes (if any) at the downstream boundary $x = X$ (see [8]).

Now, we calculate the eigenvalues $\lambda_r(\eta_k)$, $r = 1, \dots, 4$, for the matrix $\mathbf{Q}(\eta_k)$. Those eigensolutions that increase to the right correspond to eigenvalues $\Re\lambda_r < 0$, and those eigensolutions that do not decrease to the left correspond to eigenvalues $\Re\lambda_r \geq 0$. Therefore, the following boundary conditions at $x = 0$ and $x = X$ may be considered to provide an exact transfer of boundary conditions (2.39) from infinity:

$$\mathbf{S}^-(\eta_k)\hat{\mathbf{u}}(0,\, \eta_k) = \mathbf{0}, \quad k = 0, \pm 1, \pm 2, \dots, \tag{2.45a}$$

$$\mathbf{S}^+(\eta_k)\hat{\mathbf{u}}(X,\, \eta_k) = \mathbf{0}, \quad k = 0, \pm 1, \pm 2, \dots. \tag{2.45b}$$

Here, $\mathbf{S}^-(\eta_k)$ and $\mathbf{S}^+(\eta_k)$ are the special rank-deficient 4×4 matrices that depend on $\mathbf{Q}(\eta_k)$, with their ranks equal to the numbers of eigenvalues $\lambda_r(\eta_k)$ with nonnegative and negative real parts, respectively. These matrices are given by

$$\mathbf{S}^-(\eta_k) = \prod_{\Re\lambda_r(\eta_k)<0} (\mathbf{Q}(\eta_k) - \lambda_r(\eta_k)\mathbf{I})\,, \tag{2.46a}$$

$$\mathbf{S}^+(\eta_k) = \prod_{\Re\lambda_r(\eta_k)\geq 0} (\mathbf{Q}(\eta_k) - \lambda_r(\eta_k)\mathbf{I})\,. \tag{2.46b}$$

Here, $\mathbf{I}$ is an identity matrix and products in (2.46) are calculated in accordance with the multiplicities of the eigenvalues. Analogous conditions will be used in section 3 while dealing with the finite-difference formulation of the AP.

Thus, the formulation of the new finite AP is now complete. Namely, we have to solve equations (2.12) for the compactly supported right-hand side $\hat{\mathbf{f}}$, $\mathrm{supp}\hat{\mathbf{f}} \subset D_{in}$, on the domain D_Y^0 (see Figure 2.1) with the periodicity boundary conditions in the y direction (Y being the value of the period) and with boundary conditions (2.45a)–(2.46a) at $x = 0$ and boundary conditions (2.45b)–(2.46b) at $x = X$. In the next section, we proceed to the finite-difference formulation of the problem and describe the numerical algorithm for setting the global DPM-based ABCs.

3. Numerical method.

3.1. Finite-difference scheme. Let us introduce a uniform Cartesian grid in $D_Y^0 \times [0,\, T]$, with h_x, h_y, and τ being the sizes of the grid in the x, y, and t directions, respectively. We designate this grid $\mathcal{N}^{0^T}$,

$$\begin{aligned}\mathcal{N}^{0^T} = \{(x_m,\, y_j, t_l) \equiv (mh_x,\, jh_y - Y/2,\, l\tau) \,|\, h_x,\ h_y,\ \tau > 0;\\ m = 0, 1, \dots, M,\ M = X/h_x; \quad j = 0, 1, \dots, 2J+1,\ 2J+1 = Y/h_y;\\ l = 0, 1, \dots, 2L+1,\ 2L+1 = T/\tau\ \}\,.\end{aligned} \tag{3.1}$$

We will construct a second-order finite-difference approximation of the system (2.3a) on the grid $\mathcal{N}^{0^T}$ (see (3.1)) using the stencil shown in Figure 3.1.

Namely, we use the first-order differences in the x and t directions and second-order central differences in the y direction, and we center the scheme with respect to

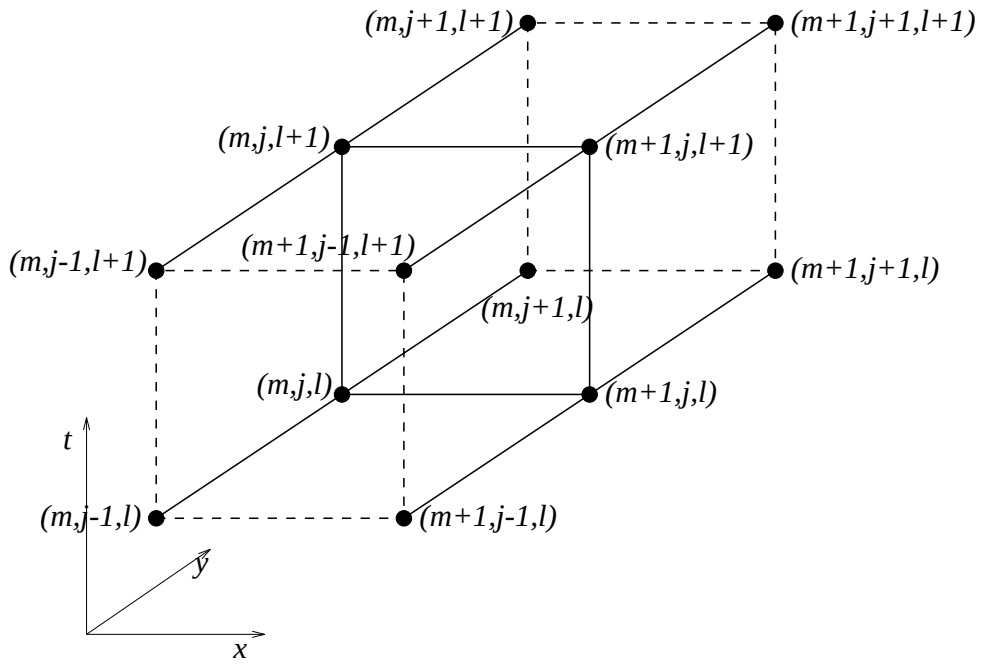

FIG. 3.1. *Stencil.*

the point $(m+1/2,\, j,\, l+1/2)$, which yields

(3.2)
$$\frac{1}{2}\mathbf{C}\left(\frac{\mathbf{u}_{m,j}^{l+1}-\mathbf{u}_{m,j}^{l}}{\tau}+\frac{\mathbf{u}_{m+1,j}^{l+1}-\mathbf{u}_{m+1,j}^{l}}{\tau}\right)+\frac{1}{2}\mathbf{D}\left(\frac{\mathbf{u}_{m+1,j}^{l+1}-\mathbf{u}_{m,j}^{l+1}}{h_x}+\frac{\mathbf{u}_{m+1,j}^{l}-\mathbf{u}_{m,j}^{l}}{h_x}\right)$$
$$+\frac{1}{4}\mathbf{F}\left(\frac{\mathbf{u}_{m,j+1}^{l}-\mathbf{u}_{m,j-1}^{l}}{2h_y}+\frac{\mathbf{u}_{m+1,j+1}^{l}-\mathbf{u}_{m+1,j-1}^{l}}{2h_y}\right.$$
$$\left.+\frac{\mathbf{u}_{m,j+1}^{l+1}-\mathbf{u}_{m,j-1}^{l+1}}{2h_y}+\frac{\mathbf{u}_{m+1,j+1}^{l+1}-\mathbf{u}_{m+1,j-1}^{l+1}}{2h_y}\right)$$
$$+\frac{1}{4}\mathbf{H}\left(\frac{\mathbf{u}_{m,j+1}^{l}-2\mathbf{u}_{m,j}^{l}+\mathbf{u}_{m,j-1}^{l}}{h_y^2}+\frac{\mathbf{u}_{m+1,j+1}^{l}-2\mathbf{u}_{m+1,j}^{l}+\mathbf{u}_{m+1,j-1}^{l}}{h_y^2}\right.$$
$$\left.+\frac{\mathbf{u}_{m,j+1}^{l+1}-2\mathbf{u}_{m,j}^{l+1}+\mathbf{u}_{m,j-1}^{l+1}}{h_y^2}+\frac{\mathbf{u}_{m+1,j+1}^{l+1}-2\mathbf{u}_{m+1,j}^{l+1}+\mathbf{u}_{m+1,j-1}^{l+1}}{h_y^2}\right)=\mathbf{0}.$$

The finite-difference scheme (3.2) is written for the nodes $m=0,\ldots,M-1$, $j=0,\ldots,2J$, $l=0,\ldots,2L$, with the assumption that we later impose periodicity boundary conditions in time as well as in the y direction. (Note that the discretization of the type (3.2) has been found to be unconditionally stable in the von Neumann sense for the corresponding scalar advection-diffusion equation.)

Then, using the periodicity conditions (compare to (2.4))

$$\mathbf{u}_{m,j}^{0}=\mathbf{u}_{m,j}^{2L+1},\quad m=0,\ldots,M,\quad j=0,\ldots,2J+1, \tag{3.3}$$

we implement the discrete Fourier transform in time (compare to (2.7) (2.6)),

(3.4)
$$\hat{\mathbf{u}}^n_{m,j} = \frac{1}{2L+1}\sum_{l=0}^{2L} \mathbf{u}^l_{m,j} e^{-inl\tau\frac{2\pi}{T}},\ m=0,\dots,M,\ j=0,\dots,2J+1,\ n=-L,\dots,L,$$

(3.5)
$$\mathbf{u}^l_{m,j} = \sum_{n=-L}^{L} \hat{\mathbf{u}}^n_{m,j} e^{inl\tau\frac{2\pi}{T}},\quad m=0,\dots,M,\ j=0,\dots,2J+1,\ l=0,\dots,2L,$$

and instead of the system (3.2), obtain

(3.6)
$$\begin{aligned}
&\frac{s_n}{2}\mathbf{C}\left(\hat{\mathbf{u}}^n_{m,j}+\hat{\mathbf{u}}^n_{m+1,j}\right) + c_n\mathbf{D}\frac{\hat{\mathbf{u}}^n_{m+1,j}-\hat{\mathbf{u}}^n_{m,j}}{h_x}\\
&\quad+\frac{c_n}{2}\mathbf{F}\left(\frac{\hat{\mathbf{u}}^n_{m,j+1}-\hat{\mathbf{u}}^n_{m,j-1}}{2h_y}+\frac{\hat{\mathbf{u}}^n_{m+1,j+1}-\hat{\mathbf{u}}^n_{m+1,j-1}}{2h_y}\right)\\
&+\frac{c_n}{2}\mathbf{H}\left(\frac{\hat{\mathbf{u}}^n_{m,j+1}-2\hat{\mathbf{u}}^n_{m,j}+\hat{\mathbf{u}}^n_{m,j-1}}{h_y^2}+\frac{\hat{\mathbf{u}}^n_{m+1,j+1}-2\hat{\mathbf{u}}^n_{m+1,j}+\hat{\mathbf{u}}^n_{m+1,j-1}}{h_y^2}\right)=\mathbf{0}.
\end{aligned}$$

Here,

$$s_n = 2i\sin\left(\frac{1}{2}n\tau\frac{2\pi}{T}\right)/\tau,\quad c_n=\cos\left(\frac{1}{2}n\tau\frac{2\pi}{T}\right),\quad n=-L,\dots,L,$$
$$m=0,\dots,M-1,\quad j=0,\dots,2J.$$

The finite-difference system (3.6) is a discrete analogue of the continuous system (2.8) on the two-dimensional grid $\mathcal{N}^0$,

(3.7)
$$\begin{aligned}
&\mathcal{N}^0=\{(x_m,\,y_j)\equiv(mh_x,\,jh_y-Y/2)\,|\,h_x,\ h_y>0;\\
&m=0,1,\dots,M,\ M=X/h_x;\quad j=0,1,\dots,2J+1,\ 2J+1=Y/h_y\,\};
\end{aligned}$$

h_x and h_y in (3.7) are the same as in (3.1).

We also note that once $\tau\longrightarrow 0$, then $s_n\longrightarrow i2\pi n/T=i\omega_n$ (see section 2) and $c_n\longrightarrow 1$.

3.2. Difference auxiliary problem. Let us construct another Cartesian grid in D^0_Y,

(3.8)
$$\begin{aligned}
&\mathcal{M}^0=\left\{(x_{m+1/2},\,y_j)\equiv((m+1/2)h_x,\,jh_y-Y/2)\,|\,h_x,\ h_y>0;\right.\\
&\left.m=0,1,\dots,M-1,\ M=X/h_x;\quad j=0,1,\dots,2J+1,\ 2J+1=Y/h_y\,\right).
\end{aligned}$$

Here, the grid sizes are the same as before. The difference AP is formulated for the inhomogeneous counterpart of (3.6) with a certain compactly supported right-hand side. The unknowns for the difference AP are defined on the grid $\mathcal{N}^0$ (see (3.7)), and the right-hand side is defined on the grid $\mathcal{M}^0$ (see (3.8)). In doing so, we obviously have the second order of approximation. We will define the specific right-hand side for the AP, $\hat{\mathbf{f}}^n_{m+1/2,j}$, $m=0,\dots,M-1$, $j=0,\dots,2J$, later on in section 3.3. For now, we provide an exact formulation of the difference AP assuming that this right-hand side is already known ($\mathrm{supp}\hat{\mathbf{f}}^n_{m+1/2,j}\subset D_{in}$).

In accordance with the results of section 2.3, we impose the periodicity boundary conditions in the y direction,

$$\hat{\mathbf{u}}^n_{m,0} = \hat{\mathbf{u}}^n_{m,2J+1}, \quad m = 0, \ldots, M, \tag{3.9}$$
$$\hat{\mathbf{u}}^n_{m,-1} = \hat{\mathbf{u}}^n_{m,2J}, \quad m = 0, \ldots, M.$$

Then, we implement the discrete Fourier transform (compare to (2.36))

$$\hat{\hat{\mathbf{u}}}^n_{m,k} = \frac{1}{2J+1} \sum_{j=0}^{2J} \hat{\mathbf{u}}^n_{m,j} e^{-ikjh_y \frac{2\pi}{Y}}, \quad m = 0, \ldots, M, \ k = -J, \ldots, J, \tag{3.10a}$$

$$\hat{\hat{\mathbf{f}}}^n_{m+1/2,k} = \frac{1}{2J+1} \sum_{j=0}^{2J} \hat{\mathbf{f}}^n_{m+1/2,j} e^{-ikjh_y \frac{2\pi}{Y}}, \quad m = 0, \ldots, M-1, k = -J, \ldots, J, \tag{3.10b}$$

and instead of the inhomogeneous counterpart to the system (3.6) obtain

$$\mathbf{A}^n_k \hat{\mathbf{u}}^n_{m+1,k} + \mathbf{B}^n_k \hat{\mathbf{u}}^n_{m,k} = \hat{\hat{\mathbf{f}}}^n_{m+1/2,k}\,, \tag{3.11}$$
$$m = 0, \ldots, M-1, \ k = -J, \ldots, J,$$

where the 4×4 matrices $\mathbf{A}^n_k$ and $\mathbf{B}^n_k$ are given by

$$\mathbf{A}^n_k = \frac{s_n}{2}\mathbf{C} + \frac{c_n}{h_x}\mathbf{D} + \frac{c_n r_k}{2}\mathbf{F} + \frac{c_n t_k}{2}\mathbf{H}, \tag{3.12}$$
$$\mathbf{B}^n_k = \frac{s_n}{2}\mathbf{C} - \frac{c_n}{h_x}\mathbf{D} + \frac{c_n r_k}{2}\mathbf{F} + \frac{c_n t_k}{2}\mathbf{H}.$$

Here,

$$r_k = i \sin\left(kh_y \frac{2\pi}{Y}\right)/h_y, \quad t_k = -4\sin^2\left(\frac{1}{2}kh_y \frac{2\pi}{Y}\right)/h_y^2,$$

and $\mathbf{C}$, $\mathbf{D}$, $\mathbf{F}$, and $\mathbf{H}$ are as defined in (2.3b). For each wavenumber k, $k = -J, \ldots, J$, (3.11) is a system of ordinary difference equations and a discrete analogue of (2.37). To find a solution to the difference AP, we will have to solve the system (3.11) for all k, $k = -J, \ldots, J$. However, the formulation of the difference AP is still incomplete. To complete it, we have to set some boundary conditions at $m = 0$ and $m = M$ (as was done at $x = 0$ and $x = X$ for the continuous case in section 2.3). These boundary conditions should guarantee the desirable far-field behavior of the solution (i.e., decay at infinity). They will be formulated separately for each wavenumber k, $k = -J, \ldots, J$, i.e., the system (3.11) will be supplemented for each k by some boundary conditions at $m = 0$ and $m = M$. The idea for constructing these boundary conditions in the discrete case is analogous to the one implemented in constructing boundary conditions (2.45), (2.46) for the continuous system (2.37). Namely, when formally considered on an infinite one-dimensional mesh, $-\infty < m < \infty$, the system (3.11) obviously becomes homogeneous at least for $m \geq M$ and $m \leq 0$. The homogeneous system has four linearly independent eigensolutions: those that correspond to $|\mu^n_r(k)| < 1$ decrease to the right (i.e., as $m \longrightarrow +\infty$), those that correspond to $|\mu^n_r(k)| > 1$ decrease to the left (i.e., as $m \longrightarrow -\infty$), and those that correspond to $|\mu^n_r(k)| = 1$ have either constant or oscillatory behavior. Here, $\mu^n_r(k)$, $r = 1, \ldots, 4$, are the eigenvalues of the matrix $\mathbf{Q}^n_k \stackrel{def}{=} (\mathbf{A}^n_k)^{-1}\mathbf{B}^n_k$. Let us note that while calculating the eigenvalues

$\mu_r(k)$ for the stationary Navier–Stokes equations [8] (the eigenvalues are calculated numerically using standard NAG subroutines), we have found that for all specific sets of the parameters involved (i.e., grid sizes h_x and h_y and hydrodynamic parameters M_0, Re, Pr, γ) the absolute values of eigenvalues were never equal to unity except for the case of zero wavenumber, $k = 0$. For $k = 0$, we have obtained a multiple eigenvalue $|\mu(0)| = 1$ (see [8]). However, even in this case, the system matrix still has a basis composed of eigenvectors, which provides us with the reason for not considering the polynomially growing solutions in [8]. For the system (3.11), we also have a particular case when the eigenvalues of the system matrix become equal to unity in absolute value. Namely, it is easy to see from (3.12) that $\mathbf{Q}_0^0 = \left(\mathbf{A}_0^0\right)^{-1}\mathbf{B}_0^0 = -\mathbf{I}$ (identity matrix). Obviously, $\mathbf{Q}_0^0$ has four linearly independent eigenvectors, so we do not have polynomially growing solutions in this case either. As for other values of k and n, a numerical check (as was done in [8]) will always be necessary to determine whether the eigenvalues $|\mu_r^n(k)| = 1$ exist. If such eigenvalues do exist, a check is also necessary to determine what their multiplicities are and if there is a basis composed of eigenvectors. Relying on our previous experience [8], we assume that while solving system (3.11), we can restrict ourselves by considering only the following two cases: $|\mu_r^n(k)| \neq 1$ and $|\mu_r^n(k)| = 1$ with the full system of eigenvectors; nontrivial Jordan blocks (of order more than one) for $|\mu_r^n(k)| = 1$ are excluded from consideration. Note that if the basis composed of eigenvectors does exist for $|\mu_r^n(k)| = 1$, then the system (3.11) will be treated in exactly the same way as in the case $|\mu_r^n(k)| \neq 1$ (the only difference is that the stability constant becomes proportional to M).

Returning to the question of setting the boundary conditions for (3.11) at $m = 0$ and $m = M$, we require that, analogous to the continuous case (see section 2.3), boundary conditions at $m = 0$ should prohibit all modes that do not decrease to the left (i.e., as $m \longrightarrow -\infty$) and boundary conditions at $m = M$ should prohibit all modes that increase to the right (i.e., as $m \longrightarrow +\infty$). Therefore, we may represent the desirable boundary conditions in the form of the matrix relations (compare to (2.45))

$$\mathbf{S}^{n-}(k)\hat{\mathbf{u}}_{0,k}^n = \mathbf{0}, \quad k = -J, \ldots, J, \tag{3.13a}$$

$$\mathbf{S}^{n+}(k)\hat{\mathbf{u}}_{M,k}^n = \mathbf{0}, \quad k = -J, \ldots, J, \tag{3.13b}$$

where

$$\mathbf{S}^{n-}(k) = \prod_{|\mu_r^n(k)|>1} \left(\mathbf{Q}_k^n - \mu_r^n(k)\mathbf{I}\right), \tag{3.14a}$$

$$\mathbf{S}^{n+}(k) = \prod_{|\mu_r^n(k)|\leq 1} \left(\mathbf{Q}_k^n - \mu_r^n(k)\mathbf{I}\right) \tag{3.14b}$$

(compare to (2.46)).

Thus, the final formulation of the difference AP is the following. One should solve the inhomogeneous counterpart to the system (3.6) in D_Y^0 on the grid $\mathcal{N}^0$ (see (3.7)), where the right-hand side $\hat{\mathbf{f}}_{m+1/2,j}^n$ is specified on the grid $\mathcal{M}^0$ (see (3.8)), $\mathrm{supp}\hat{\mathbf{f}}_{m+1/2,j}^n \subset D_{in}$, with periodicity boundary conditions (3.9) in the y direction and boundary conditions (3.13a)–(3.14a) at the line $m = 0$ and (3.13b)–(3.14b) at the line $m = M$.

To solve the difference AP, we implement the following numerical procedure. First, apply the discrete Fourier transform (3.10) to both sides of the finite-difference

system; then solve the system of ordinary difference equations (3.11) with the boundary conditions (3.13) for each wavenumber k, $k = -J, \ldots, J$; and finally, restore the solution by means of the inverse Fourier transform

$$\hat{\mathbf{u}}^n_{m,j} = \sum_{k=-J}^{k=J} \hat{\hat{\mathbf{u}}}^n_{m,k} e^{ikjh_y \frac{2\pi}{Y}}, \quad m = 0, \ldots, M, \ j = 0, \ldots, 2J. \tag{3.15}$$

The type of boundary conditions (3.13) (which are imposed separately for each wavenumber k) makes this choice of numerical method most relevant. An effective algorithm for solving one-dimensional problems (3.11)–(3.13) is delineated in our work [27]. We do not reproduce the corresponding results here, we only note that this algorithm may be thought of as a version of the well-known successive substitution technique, but without its "inverse" or "resolving" part. The computational cost of the numerical procedure of [27] as applied to solving the problem (3.11)–(3.13) is $\mathcal{O}(M)$ operations (for each k, $k = -J, \ldots, J$).

Let us now briefly describe the concept of convergence for the solutions of the difference AP. According to section 2.3, we approximate the nonperiodic solution by a periodic one on a finite interval $-\breve{y} \le y \le \breve{y}$ when the period Y grows, $Y \longrightarrow +\infty$. In its own turn, an approximate solution to the periodic problem is found by a finite-difference method on the grid with sizes h_x and h_y. Therefore, we will consider (uniform) convergence of the periodic difference solution (i.e., solution of the difference AP) to the nonperiodic continuous solution (i.e., to the solution of the original continuous AP) only on a finite rectangle $(0, X) \times (-\breve{y}, \breve{y})$ (this rectangle should be large enough to contain at least Γ_1) rather than on the whole domain of the difference AP. Moreover, we will consider this convergence not only when the grid size vanishes, but also when the period Y synchronously increases; i.e., as $(h_x, h_y, Y) \longrightarrow (0, 0, +\infty)$. Of course, the rate of decrease for the grid sizes h_x and h_y and the rate of increase for the period Y are not independent; some estimates connecting these rates can be found in [8]. Furthermore, some numerical experiments from [8] show that the presented construction of the difference AP does ensure the convergence of its solution to the solution of the continuous AP in the sense described above.

3.3. Computation of the ABCs. In accordance with section 2.1, to set the ABCs, we need to know the following data: $(\hat{\mathbf{u}}^n_\nu, \frac{\partial \hat{\mathbf{u}}^n_\nu}{\partial \zeta})$; here, ζ is the normal to Γ. When integrating the Navier–Stokes equations step by step in time, we assume that $(\hat{\mathbf{u}}^n_\nu, \frac{\partial \hat{\mathbf{u}}^n_\nu}{\partial \zeta})$ is provided from inside D_{in}; then we use these data to restore $\hat{\mathbf{u}}^n_{\nu_1}$, which enables us to advance the next time step. However, as we carry out our analysis in the Fourier space, we cannot consider $(\hat{\mathbf{u}}^n_\nu, \frac{\partial \hat{\mathbf{u}}^n_\nu}{\partial \zeta})$ as the actual values obtained inside the computational domain. To get $(\hat{\mathbf{u}}^n_\nu, \frac{\partial \hat{\mathbf{u}}^n_\nu}{\partial \zeta})$, we first have to Fourier-transform the function $(\mathbf{u}_\nu, \frac{\partial \mathbf{u}_\nu}{\partial \zeta})$. Without loss of generality, we may always think that the latter is specified at the following nodes:

$$\nu \times \{\tau l \mid l = 0, \ldots, 2L+1, \ \tau(2L+1) = T\}. \tag{3.16}$$

Of course, actual discretization in time for the Navier–Stokes equations inside D^T_{in} should not necessarily coincide with the one used for the solution of the exterior linearized problem (see (3.1)). However, we may always use some interpolation in time to obtain the boundary data on the mesh (3.16) that is uniform with respect to t. Hereafter, we simply assume that this interpolation (which is one dimensional in

time and of sufficiently high order) has already been implemented for each node ν, if necessary.

Another important issue related to the step by step integration in time is that the function $(\mathbf{u}_\nu,\ \frac{\partial \mathbf{u}_\nu}{\partial \zeta})$, which provides the boundary data, is not necessarily time-periodic until we achieve a true oscillatory regime. However, for the purpose of constructing the ABCs, we will propose some generalized treatment of the boundary data as being already periodic. Namely, let us formally calculate the Fourier coefficients of $(\mathbf{u}_\nu,\ \frac{\partial \mathbf{u}_\nu}{\partial \zeta})$,

$$\left(\hat{\mathbf{u}}_\nu^n,\ \frac{\partial \hat{\mathbf{u}}_\nu^n}{\partial \zeta}\right) = \frac{1}{2L+1}\sum_{l=1}^{2L+1}\left(\mathbf{u}_\nu^l,\ \frac{\partial \mathbf{u}_\nu^l}{\partial \zeta}\right) e^{-inl\tau\frac{2\pi}{T}}, \quad n=-L,\dots,L. \tag{3.17}$$

Then, it is well known (see, e.g., [28] by Kolmogorov and Fomin) that the time-periodic function

$$\left(\mathbf{v}_\nu^l,\ \frac{\partial \mathbf{v}_\nu^l}{\partial \zeta}\right) = \sum_{n=-L}^{L}\left(\hat{\mathbf{u}}_\nu^n,\ \frac{\partial \hat{\mathbf{u}}_\nu^n}{\partial \zeta}\right) e^{inl\tau\frac{2\pi}{T}}, \quad l=0,\dots,2L+1, \tag{3.18}$$

minimizes the functional

$$\left\|\left(\mathbf{u}_\nu,\ \frac{\partial \mathbf{u}_\nu}{\partial \zeta}\right) - \left(\mathbf{v}_\nu,\ \frac{\partial \mathbf{v}_\nu}{\partial \zeta}\right)\right\|_2$$

($\|\cdot\|_2$ is a usual Euclidean norm) on the class of periodic functions; i.e., $(\mathbf{v}_\nu,\ \frac{\partial \mathbf{v}_\nu}{\partial \zeta})$ from formula (3.18) is the best periodic approximation of $(\mathbf{u}_\nu,\ \frac{\partial \mathbf{u}_\nu}{\partial \zeta})$ in the sense of least squares. Relying on this property, we will further use the Fourier coefficients (3.17) as the boundary data that "drive" the ABCs (which may be referred to as the generalized treatment of the boundary data as being time-periodic). As we integrate the Navier–Stokes equations in time and approach the true oscillatory regime, the "source" function $(\mathbf{u}_\nu,\ \frac{\partial \mathbf{u}_\nu}{\partial \zeta})$ and its Fourier series $(\mathbf{v}_\nu,\ \frac{\partial \mathbf{v}_\nu}{\partial \zeta})$ (see (3.18)) also approach each other.

We now implement the DPM [9, 10, 11] to actually calculate the ABCs. We note that the boundary data $(\hat{\mathbf{u}}_\nu^n,\ \frac{\partial \hat{\mathbf{u}}_\nu^n}{\partial \zeta})$ are specified on the curve Γ, which is positioned arbitrarily with respect to coordinate lines of the grid $\mathcal{N}^0$; see (3.7). Moreover, we do not impose any restrictions on the shape of Γ itself. In our opinion, the DPM [9, 10, 11] provides an ideal tool for treating such geometrically complicated problems.

Let us introduce the following discrete sets. We consider a six-node two-dimensional stencil

$$\begin{aligned} &St_{m+1/2,j} \\ &\quad = \{(x_m,\ y_j),\ (x_m,\ y_{j+1}),\ (x_m,\ y_{j-1}),\ (x_{m+1},\ y_j),\ (x_{m+1},\ y_{j+1}),\ (x_{m+1},\ y_{j-1})\}. \end{aligned}$$

This stencil is actually a projection of the one from Figure 3.1 onto the plane $t = \text{const}$. Obviously, the discretization (3.6) was obtained using $St_{m+1/2,j}$. Then, we define

$$\begin{aligned} &\mathcal{M}_{in} = \mathcal{M}^0 \bigcap D_{in}, && \mathcal{M} = \mathcal{M}^0 \backslash \mathcal{M}_{in}, \\ &\mathcal{N}_{in} = \bigcup_{(x_{m+1/2},\ y_j)\in\mathcal{M}_{in}} St_{m+1/2,j}, && \mathcal{N} = \bigcup_{(x_{m+1/2},\ y_j)\in\mathcal{M}} St_{m+1/2,j}, \\ &\gamma = \mathcal{N} \bigcap \mathcal{N}_{in}. \end{aligned}$$

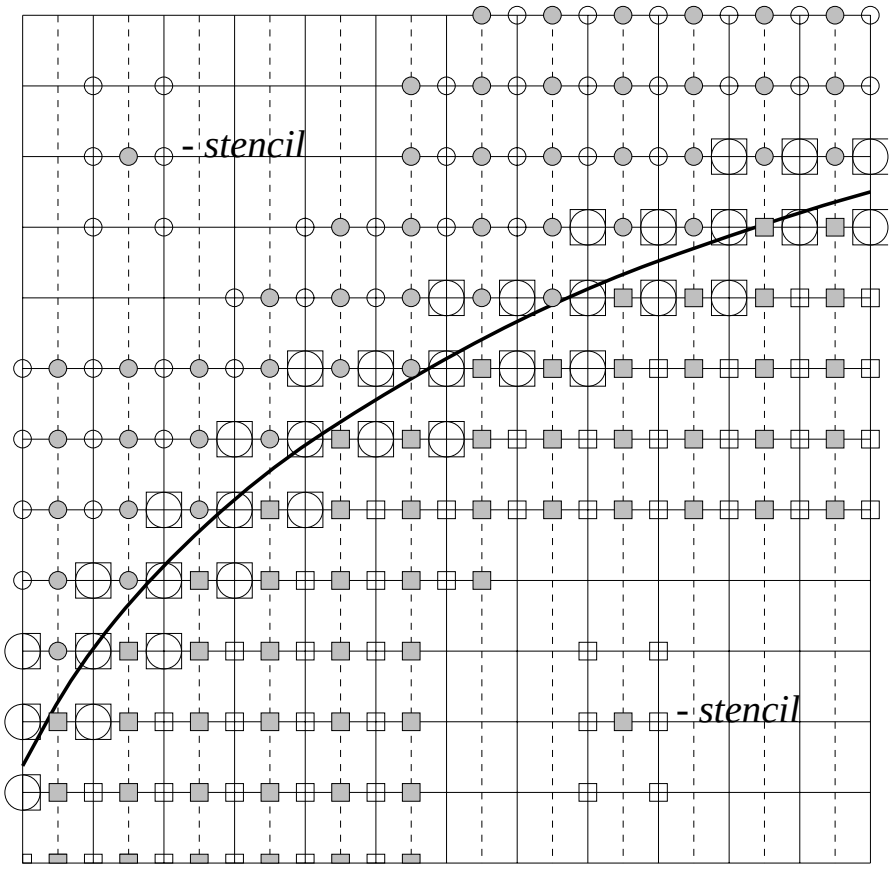

FIG. 3.2. *Grid sets. Grid $\mathcal{N}^0$: continuous thin lines; grid $\mathcal{M}^0$: continuous thin horizontal lines and dashed thin vertical lines; continuous boundary Γ: thick dark line; $\mathcal{M}_{in}$: grey boxes; $\mathcal{M}$: grey circles; $\mathcal{N}_{in}$: white boxes; $\mathcal{N}$: white circles; $\gamma = \mathcal{N} \bigcap \mathcal{N}_{in}$: big white circles and boxes.*

Clearly, the set of grid nodes γ is located near the artificial boundary Γ; we will call this set *the grid boundary*. The sets $\mathcal{M}_{in}$, $\mathcal{M}$, $\mathcal{N}_{in}$, $\mathcal{N}$, and γ are shown in Figure 3.2.

Further, we will need to interpolate the grid functions from $\mathcal{N}^0$ to the points $\nu_1 \subset \Gamma_1$. Let us select all those nodes $\kappa \subset \mathcal{N}^0$ that should be taken into account once constructing local interpolation formulas of sufficiently high (e.g., second) order. All the nodes κ are obviously located not far from Γ_1. Without loss of generality, we may always assume that $\kappa \subset \mathcal{N}$. We denote the operation of local interpolation from $\kappa \subset \mathcal{N}$ to ν_1 by $\mathbf{R}_{\nu_1 \kappa}$.

Let us also introduce the set of collocation points $\sigma \subset \Gamma$ and the space of eight-component vector functions $\hat{\mathbf{W}}^n_\sigma \ni \hat{\mathbf{w}}^n_\sigma$ defined on the set σ. The elements of $\hat{\mathbf{W}}^n_\sigma$ will be used to calculate the density of the generalized potential. Henceforth, we will treat $\hat{\mathbf{w}}^n_\sigma$ as vectors containing the values of $\hat{u}^n$, $\hat{v}^n$, $\hat{p}^n$, $\hat{\rho}^n$ and the values of the derivatives

$$\frac{\partial \hat{u}^n}{\partial \zeta}, \frac{\partial \hat{v}^n}{\partial \zeta}, \frac{\partial \hat{p}^n}{\partial \zeta}, \frac{\partial \hat{\rho}^n}{\partial \zeta}$$

at the points σ; here, ζ is the (outward) normal to Γ. Note that the functions $\hat{\mathbf{w}}^n_\sigma$ are the discrete approximations of $(\hat{\mathbf{u}}^n_\Gamma, \frac{\partial \hat{\mathbf{u}}^n_\Gamma}{\partial \zeta})$ from section 2.1.

Generally, the sizes h_x and h_y of the grid $\mathcal{N}^0$ and the size h_σ of the one-dimensional collocation grid on the curve Γ are not independent. Some theoretical questions concerning the correlation between the sizes of the grids $\mathcal{N}^0$ and σ are delineated in [9] for certain versions of the DPM algorithm. As for practical applications, the final choice of grids is always done taking into account some previous computational results. In particular, it seems useful to conduct the computations (see [12, 13]) for the set of collocation points, which is more concentrated at the outflow part of the external boundary in the wake region and uniformly spaced at the inflow part of the external boundary. Moreover, sometimes the relation $|\sigma| \sim |\gamma|^{1/2}$ appears proper. At any rate, for each specific class of problems (determined both by the geometry of computational domain and by the parameters of fluid at infinity), one always can make an appropriate choice of the grids $\mathcal{N}^0$ and σ relying on general theory [9] and on the numerical experience.

Let us now specify some $\hat{\mathbf{w}}^n_\sigma \in \hat{\mathbf{W}}^n_\sigma$ and implement the following procedure. First, we smoothly interpolate $\hat{\mathbf{w}}^n_\sigma$ along Γ (i.e., along the smooth components of Γ) and obtain the function $\mathbf{R}\hat{\mathbf{w}}^n_\sigma$; here, $\mathbf{R}$ is an interpolation operator. Then, we drop the normals from the nodes γ to Γ and find the values of $\mathbf{R}\hat{\mathbf{w}}^n_\sigma$ at the foot of each normal. Since $\hat{\mathbf{w}}^n_\sigma$ (and consequently, $\mathbf{R}\hat{\mathbf{w}}^n_\sigma$) contains the values of both $\hat{u}^n$, $\hat{v}^n$, $\hat{p}^n$, $\hat{\rho}^n$ and their normal derivatives, and since the distance between any node γ and the curve Γ is small (of order h), we may approximately find $\hat{u}^n$, $\hat{v}^n$, $\hat{p}^n$, $\hat{\rho}^n$ at the nodes γ using the first two terms of the Taylor expansion. We will designate the entire operation of continuation of the boundary data from σ to γ as $\pi_{\gamma\sigma}$, $\pi_{\gamma\sigma}\hat{\mathbf{w}}^n_\sigma = \hat{\mathbf{u}}^n_\gamma$. Note that the above algorithm of continuation applies only to the smooth parts of Γ (where the normal exists). In practice, however, the curve Γ is usually not smooth (see Figure 2.1), and it is impossible to construct an appropriate normal when the node γ is located in some neighborhood of the "corner" point of the curve. The construction of the operator $\pi_{\gamma\sigma}$ in this case is based on the existence of two linearly independent directions along the curve, which enables us to obtain the desirable continuation anyway.

Now, using the calculated continuation of the boundary data, $\hat{\mathbf{u}}^n_\gamma = \pi_{\gamma\sigma}\hat{\mathbf{w}}^n_\sigma$, we construct the following grid function:

$$\hat{\mathbf{u}}^n_{\mathcal{N}^0}\Big|_{m,j} = \begin{cases} \hat{\mathbf{u}}^n_\gamma\Big|_{m,j}, & \text{if} \quad (x_m,\, y_j) \in \gamma, \\ \mathbf{0}, & \text{if} \quad (x_m,\, y_j) \in \mathcal{N}^0 \backslash \gamma, \end{cases} \tag{3.19}$$

which is defined already on the entire grid $\mathcal{N}^0$; see (3.7). Then we substitute the function $\hat{\mathbf{u}}^n_{\mathcal{N}^0}$ from the formula (3.19) into the left-hand side of the system (3.6). Generally speaking, $\hat{\mathbf{u}}^n_{\mathcal{N}^0}$ does not satisfy equations (3.6), so we generate some nonzero right-hand side, which we designate $\mathbf{L}^n_0\, \hat{\mathbf{u}}^n_{\mathcal{N}^0}$. Here, $\mathbf{L}^n_0$ is the linear operator defined by the left-hand side of the system (3.6). (The operator $\mathbf{L}^n_0$ takes the functions defined on the grid $\mathcal{N}^0$ (see (3.7)) as input and generates the functions defined on the grid $\mathcal{M}^0$ (see (3.8)) as a result.) Finally, we truncate the function $\mathbf{L}^n_0\, \hat{\mathbf{u}}^n_{\mathcal{N}^0}$ to the set $\mathcal{M}_{in}$, which yields

$$\hat{\mathbf{f}}^n_{\mathcal{M}^0}\Big|_{m+1/2,j} = \begin{cases} \mathbf{L}^n_0\, \hat{\mathbf{u}}^n_{\mathcal{N}^0}\Big|_{m+1/2,j}, & \text{if} \quad (x_{m+1/2},\, y_j) \in \mathcal{M}_{in}, \\ \mathbf{0}, & \text{if} \quad (x_{m+1/2},\, y_j) \notin \mathcal{M}_{in}. \end{cases} \tag{3.20}$$

We will use the function $\hat{\mathbf{f}}^n_{\mathcal{M}^0} \equiv \hat{\mathbf{f}}^n_{m+1/2,j}$ *from the formula* (3.20) *as the right-hand side for the difference AP;* by definition, $\operatorname{supp}\hat{\mathbf{f}}^n_{m+1/2,j} \subset D_{in}$. Once we solve the difference

AP with the right-hand side $\hat{\mathbf{f}}^n_{\mathcal{M}^0}$ (see (3.20)), we get the function $\mathbf{G}^n_0\,\hat{\mathbf{f}}^n_{\mathcal{M}^0}$. Here, $\mathbf{G}^n_0$ is the Green (i.e., inverse) operator of the difference AP. The function $\mathbf{G}^n_0\,\hat{\mathbf{f}}^n_{\mathcal{M}^0}$ is defined on the grid $\mathcal{N}^0$. Being considered only on the subgrid $\mathcal{N} \subset \mathcal{N}^0$, it is called *the difference potential* with the density $\hat{\mathbf{u}}^n_\gamma$, $\mathbf{P}^n_{\mathcal{N}\gamma}\hat{\mathbf{u}}^n_\gamma = \mathbf{G}^n_0\,\hat{\mathbf{f}}^n_{\mathcal{M}^0}|_{\mathcal{N}}$ [9, 10, 11]. Clearly, the difference potential satisfies equations (3.6), since $\hat{\mathbf{f}}^n_{\mathcal{M}^0} = \mathbf{0}$ on $\mathcal{M}$; moreover, it satisfies the boundary conditions of the difference AP. The difference potential $\mathbf{P}^n_{\mathcal{N}\gamma}\hat{\mathbf{u}}^n_\gamma$ is a discrete realization of the generalized potential mentioned in section 1. Later, we will find an approximate (i.e., difference) solution to the problem (2.8)–(2.9)–(2.10) in the form of a difference potential and then use this solution to construct the ABCs, i.e., to obtain the missing relations between the unknowns at $\nu \subset \Gamma$ and at $\nu_1 \subset \Gamma_1$.

Having calculated the difference potential on γ, we can then construct the operator $\mathbf{P}^n_\gamma$ as the trace of the potential, $\mathbf{P}^n_\gamma\hat{\mathbf{u}}^n_\gamma \stackrel{def}{=} \mathbf{P}^n_{\mathcal{N}\gamma}\hat{\mathbf{u}}^n_\gamma|_\gamma$; this operator is generally the key element of any DPM-based approach. Actually, $\mathbf{P}^n_\gamma$ is a difference boundary projection, $\left(\mathbf{P}^n_\gamma\right)^2 = \mathbf{P}^n_\gamma$ [9, 10, 11], which substitutes $\mathbf{P}^n_\Gamma$ (see section 2.1, equation (2.11)) into practical computations.

We now formulate the main result of the DPM theory [9, 10, 11]. Consider the entire space of grid functions $\hat{\mathbf{u}}^n_\gamma$ defined on γ. Those and only those elements of this space that satisfy the equation

$$\mathbf{P}^n_\gamma\hat{\mathbf{u}}^n_\gamma = \hat{\mathbf{u}}^n_\gamma \tag{3.21}$$

can be complemented to $\mathcal{N}$ so that the complement solves the system (3.6) with boundary conditions (3.9), (3.13). The projection $\mathbf{P}^n_\gamma$ can be thought of as a discrete analogue of the Calderon boundary pseudodifferential operators [20].

Thus, equation (3.21) provides for an exhaustive classification of all those and only those grid densities $\hat{\mathbf{u}}^n_\gamma$ that are traces of some solution to (3.6)–(3.9)–(3.13) on $\mathcal{N}$. Therefore, we have equivalently replaced the linear system (3.6) on $\mathcal{N}$, along with the boundary conditions (3.9), (3.13), by the boundary equation with projection (3.21). Consequently, we can now specify the proper boundary data (see (2.10)) for the discrete counterpart of the problem (2.8)–(2.9)–(2.10). Namely, let $(\hat{\mathbf{u}}^n_\nu, \frac{\partial\hat{\mathbf{u}}^n_\nu}{\partial\zeta})$ be provided from inside D_{in}. We interpolate this function along Γ to the set of collocation points σ, $\hat{\mathbf{w}}^n_\sigma = \mathbf{R}_{\sigma\nu}(\hat{\mathbf{u}}^n_\nu, \frac{\partial\hat{\mathbf{u}}^n_\nu}{\partial\zeta})$, and then continue $\hat{\mathbf{w}}^n_\sigma$ to γ using the operator $\pi_{\gamma\sigma}$. Finally, we apply $\mathbf{P}^n_\gamma$. In accordance with the main result formulated above, the grid function

$$\hat{\mathbf{v}}^n_\gamma = \mathbf{P}^n_\gamma\pi_{\gamma\sigma}\mathbf{R}_{\sigma\nu}\left(\hat{\mathbf{u}}^n_\nu,\ \frac{\partial\hat{\mathbf{u}}^n_\nu}{\partial\zeta}\right) \tag{3.22}$$

admits the complement to $\mathcal{N}$ that solves (3.6)–(3.9)–(3.13).

We now proceed to the second stage of constructing the ABCs. Instead of the problem (2.8)–(2.9)–(2.10), we will consider its discrete counterpart: to solve (3.6) on $\mathcal{N}$ with external boundary conditions (3.9)–(3.13) and with boundary condition

$$\hat{\mathbf{u}}^n_\gamma = \hat{\mathbf{v}}^n_\gamma \tag{3.23}$$

at γ; $\hat{\mathbf{v}}^n_\gamma$ in equality (3.23) comes from (3.22). The solvability of the problem (3.6)–(3.9)–(3.13)–(3.23) is guaranteed by the special type of boundary data provided in the formula (3.22).

To actually find the solution to the problem (3.6)–(3.9)–(3.13)–(3.23), we calculate the difference potential $\mathbf{P}^n_{\mathcal{N}\gamma}\hat{\mathbf{v}}^n_\gamma$ with the density $\hat{\mathbf{v}}^n_\gamma$ from the formula (3.22), which

requires solving the AP. Since we eventually need to know this solution only on ν_1, it is sufficient to calculate the potential only at κ and then interpolate: $\hat{\mathbf{u}}^n_{\nu_1} = \mathbf{P}^n_{\nu_1\gamma}\hat{\mathbf{v}}^n_\gamma = \mathbf{R}_{\nu_1\kappa}\mathbf{P}^n_{\kappa\gamma}\hat{\mathbf{v}}^n_\gamma$. Finally, we obtain

$$\hat{\mathbf{u}}^n_{\nu_1} = \mathbf{R}_{\nu_1\mathcal{N}}\mathbf{P}^n_{\mathcal{N}\gamma}\mathbf{P}^n_\gamma\pi_{\gamma\sigma}\mathbf{R}_{\sigma\nu}\left(\hat{\mathbf{u}}^n_\nu,\ \frac{\partial\hat{\mathbf{u}}^n_\nu}{\partial\zeta}\right). \tag{3.24}$$

In fact, it is possible to show that for the actual computations the operator $\mathbf{P}^n_\gamma$ can be eliminated from the sequence of operators in the formula (3.24) (which combines two stages in calculating the ABCs into one). Indeed, it is proven in [9] that for any grid density $\hat{\mathbf{v}}^n_\gamma$: $\mathbf{P}^n_{\mathcal{N}\gamma}\mathbf{P}^n_\gamma\hat{\mathbf{v}}^n_\gamma = \mathbf{P}^n_{\mathcal{N}\gamma}\hat{\mathbf{v}}^n_\gamma$. Therefore,

$$\hat{\mathbf{u}}^n_{\nu_1} = \mathbf{R}_{\nu_1\mathcal{N}}\mathbf{P}^n_{\mathcal{N}\gamma}\pi_{\gamma\sigma}\mathbf{R}_{\sigma\nu}\left(\hat{\mathbf{u}}^n_\nu,\ \frac{\partial\hat{\mathbf{u}}^n_\nu}{\partial\zeta}\right) \overset{def}{=} \hat{\mathbf{T}}^n\left(\hat{\mathbf{u}}^n_\nu,\ \frac{\partial\hat{\mathbf{u}}^n_\nu}{\partial\zeta}\right). \tag{3.25}$$

Equality (3.25) provides the missing relations between the unknowns at ν and at ν_1 in the Fourier space; these relations are based on the solution to the linearized exterior problem. We emphasize that to obtain (3.25) we need to calculate the solution to the difference AP only at κ, i.e., on some neighborhood of D_{in}. Therefore, the consideration of convergence only on a fixed interval $-\breve{y} \le y \le \breve{y}$ (as stated in section 2.3) is now justified.

We also note that the entire algorithm becomes most convenient from a practical standpoint if we calculate the matrix representation of the operator $\hat{\mathbf{T}}^n$ from (3.25). To do that, we choose some basis in $\hat{\mathbf{W}}^n_\sigma$, e.g., the simplest one, composed of the vectors like $(0, \dots, 0, 1, 0, \dots, 0)$ and implement the entire procedure described above. More precisely, we calculate $\hat{\mathbf{u}}^n_{\nu_1} = \mathbf{R}_{\nu_1\kappa}\mathbf{P}^n_{\kappa\gamma}\pi_{\gamma\sigma}\hat{\mathbf{w}}^n_\sigma$ for each basis vector $\hat{\mathbf{w}}^n_\sigma$. In so doing, we obtain the matrix of $\mathbf{R}_{\nu_1\kappa}\mathbf{P}^n_{\kappa\gamma}\pi_{\gamma\sigma}$ (each column will be the response to a specific basic function $\hat{\mathbf{w}}^n_\sigma$) and then, multiplying the above matrix from the right by the interpolation matrix $\mathbf{R}_{\sigma\nu}$, we finally obtain the matrix representation of $\hat{\mathbf{T}}^n$. (Note that we do not start from basis functions on the nodes ν since the number of nodes σ is usually much less than the number of nodes ν.) Clearly, the computation of each column of the matrix $\mathbf{R}_{\nu_1\kappa}\mathbf{P}^n_{\kappa\gamma}\pi_{\gamma\sigma}$ requires solving the difference AP once per basis vector, which, in turn, involves the direct (3.10b) and inverse (3.15) Fourier transforms and the solution of (3.11)–(3.13) for each wavenumber k, $k = -J, \dots, J$. Either Fourier transform will require here only $\mathcal{O}(M \cdot J)$, rather than $\mathcal{O}(M \cdot J^2)$ operations (for definitions of M and J, see (3.1)). Indeed, the support of the right-hand side $\hat{\mathbf{f}}^n_{\mathcal{M}^0}$ is actually concentrated near Γ since $\hat{\mathbf{u}}^n_{\mathcal{N}^0}$ differs from zero only on γ and the operator $\mathbf{L}^n_0$ is local. Therefore, while calculating the direct Fourier transform (3.10b) for each m, $m = 0, \dots, M-1$, only a few values $\hat{\mathbf{f}}^n_{m+1/2,j}$ differ from zero and consequently, the total cost of this computation is $\mathcal{O}(M \cdot J)$ operations. Analogously, while calculating the inverse Fourier transform (3.15) for each m, $m = 0, \dots, M$, we need to know $\hat{\mathbf{u}}^n_{m,j}$ only for a few selected values of j since all other (x_m, y_j) do not belong to κ. Therefore, the total cost of this computation is $\mathcal{O}(M \cdot J)$ operations as well. Finally, the solution of (3.11)–(3.13) for each wavenumber k, $k = -J, \dots, J$, costs $\mathcal{O}(M)$ operations (see section 3.2). Adding all these quantities, we obtain a total of $\mathcal{O}(M \cdot J)$ operations for the computation of each column of the matrix $\mathbf{R}_{\nu_1\kappa}\mathbf{P}^n_{\kappa\gamma}\pi_{\gamma\sigma}$. We see that though the entire algorithm requires repeated solution of the difference AP, this solution may be obtained by means of an efficient procedure, which makes the total expense for calculating the ABCs quite acceptable.

Recall that our final goal is to express the values of physical variables at ν_1, $\mathbf{u}_{\nu_1} \equiv (u_{\nu_1}, v_{\nu_1}, p_{\nu_1}, \rho_{\nu_1})$, in terms of $(\mathbf{u}_\nu, \frac{\partial\mathbf{u}_\nu}{\partial\zeta})$. Choosing the same discretization in

time as (3.16) and implementing the inverse Fourier transform (see (3.18)), we obtain from (3.25)

$$\mathbf{u}^l_{\nu_1} = \sum_{n=-L}^{n=L} \hat{\mathbf{T}}^n \left(\hat{\mathbf{u}}^n_\nu,\ \frac{\partial \hat{\mathbf{u}}^n_\nu}{\partial \zeta} \right) e^{inl\tau \frac{2\pi}{T}}, \quad l = 0, \ldots, 2L+1. \tag{3.26}$$

Then, substituting (3.17) into (3.26) and changing the summation order, we get

$$\begin{aligned} \mathbf{u}^l_{\nu_1} &= \sum_{n=-L}^{n=L} \hat{\mathbf{T}}^n e^{inl\tau \frac{2\pi}{T}} \frac{1}{2L+1} \sum_{s=1}^{2L+1} \left(\mathbf{u}^s_\nu,\ \frac{\partial \mathbf{u}^s_\nu}{\partial \zeta} \right) e^{-ins\tau \frac{2\pi}{T}} \\ &= \frac{1}{2L+1} \sum_{n=-L}^{n=L} \sum_{s=1}^{2L+1} \hat{\mathbf{T}}^n e^{inl\tau \frac{2\pi}{T}} \left(\mathbf{u}^s_\nu,\ \frac{\partial \mathbf{u}^s_\nu}{\partial \zeta} \right) e^{-ins\tau \frac{2\pi}{T}} \\ &= \sum_{s=1}^{2L+1} \left(\frac{1}{2L+1} \sum_{n=-L}^{n=L} e^{in(l-s)\tau \frac{2\pi}{T}} \hat{\mathbf{T}}^n \right) \left(\mathbf{u}^s_\nu,\ \frac{\partial \mathbf{u}^s_\nu}{\partial \zeta} \right). \end{aligned}$$

Finally, designating

$$\mathbf{T}^{l,s} = \left(\frac{1}{2L+1} \sum_{n=-L}^{n=L} e^{in(l-s)\tau \frac{2\pi}{T}} \hat{\mathbf{T}}^n \right), \quad l = 0, \ldots, 2L+1,$$

we obtain

$$\mathbf{u}^l_{\nu_1} = \sum_{s=1}^{2L+1} \mathbf{T}^{l,s} \left(\mathbf{u}^s_\nu,\ \frac{\partial \mathbf{u}^s_\nu}{\partial \zeta} \right), \quad l = 0, \ldots, 2L+1. \tag{3.27}$$

Equality (3.27), which is a specification of (2.11), provides the missing boundary relations between the values of the unknowns at Γ^T and at Γ_1^T (in the discrete formulation). Therefore, equality (3.27) is actually the ABCs we were aiming to obtain. We additionally note that equality (3.27) can be simplified for the case of integrating the Navier–Stokes equations step by step in time inside D_{in}. Indeed, in doing so, we actually need to know $\mathbf{u}_{\nu_1}$ only on the upper time level, i.e., for $t = T$ (see above), which corresponds to $l = 2L+1$ or to $l = 0$ because of the periodicity. Substituting $l = 0$ into (3.27), we obtain

$$\mathbf{u}_{\nu_1}\Big|_{t=T} = \sum_{s=1}^{2L+1} \mathbf{T}^{0,s} \left(\mathbf{u}^s_\nu,\ \frac{\partial \mathbf{u}^s_\nu}{\partial \zeta} \right). \tag{3.28}$$

Equality (3.28) is the desired global ABC for implementation together with the step by step integration procedure in time. Indeed, (3.28) expresses the values of u, v, p, and ρ (perturbations) at the outermost coordinate row ν_1 on the upper time level $t = T$ as a function of the prescribed data $(\mathbf{u}_\nu, \frac{\partial \mathbf{u}_\nu}{\partial \zeta})|_{\Gamma^T}$ through the time-periodic solution of the linearized thin-layer equations with the free-stream boundary condition at infinity. We note that the matrices of operators $\mathbf{T}^{0,s}$ are calculated explicitly and therefore, practical implementation of ABCs (3.28) is reduced to several matrix–vector multiplications. We also note that this practical implementation may preliminarily require some interpolation in time at the nodes ν. If we use an explicit scheme for integrating the Navier–Stokes equations inside D_{in}, then we directly implement (3.28)

at each time step for determining the missing values of the unknowns at the outermost coordinate row of the grid on the upper time level. If the scheme inside D_{in} is implicit, then we include the relations (3.28) into the system of equations we solve on the upper time level, treating all $\mathbf{T}^{0,s}(\mathbf{u}^s_\nu, \frac{\partial \mathbf{u}^s_\nu}{\partial \zeta})$ for $s < 2L+1$ as forcing terms.

4. Concluding remarks. We have constructed the DPM-based nonlocal ABCs for computation of oscillating external flows, specifically, compressible viscous fluid flows past finite bodies. The ABCs are developed using the difference potentials [9, 10, 11] for the thin layer governing equations linearized in the far field. To justify the constructions of difference potentials, we provide some results on solvability of the linearized thin-layer equations. The nonlocal nature of the ABCs proposed above arises from their closeness to the exact boundary conditions. In spite of this nonlocal nature, the DPM-based ABCs apply to artificial boundaries of irregular shape with equal ease, which is very important for applications.

In comparison with our previous work [8, 12, 13], the ABCs proposed above have two major differences. Foremost is the fact that, in this paper, we study time-periodic rather than steady-state problems, which is an extension from the standpoint of physics. From the standpoint of numerics, the algorithm described above also differs markedly from the previous versions of the DPM-based ABCs. The latter difference remains even if we apply this algorithm to a steady-state problem, which formally means letting $n = 0$, $\omega_n = 0$ everywhere starting from (2.8) and, therefore, results in retaining only one term that corresponds to $s = 2L+1$ in (3.28):

$$\mathbf{u}_{\nu_1} = \mathbf{T}\left(\mathbf{u}_\nu, \frac{\partial \mathbf{u}_\nu}{\partial \zeta}\right) \tag{4.1}$$

(the superscripts are omitted). The difference between boundary conditions (4.1) and the ABCs from [8, 12, 13] is that (4.1) is based on the thin-layer equations and the direct implementation of the projection $\mathbf{P}^n_\gamma$ from (3.21) (for $n = 0$), whereas in [8, 12, 13] we substitute $\mathbf{u}_\gamma = \pi_{\gamma\sigma}\mathbf{R}_{\sigma\nu}(\mathbf{u}_\nu, \frac{\partial \mathbf{u}_\nu}{\partial \zeta})$ into the boundary equation with projection obtained for the central-difference discretization of the linearized full Navier–Stokes equations and solve the resulting equation (by means of a certain variational approach) with respect to $\frac{\partial \mathbf{u}_\nu}{\partial \zeta}$, assuming that $\mathbf{u}_\nu$ is known. This operation is analogous to computation of the Dirichlet-to-Neumann maps or Poincaré–Steklov operators. In so doing, we obtain (see [8, 12, 13]) the ABCs in the form

$$\mathbf{u}_{\nu_1} = \mathbf{T}'\mathbf{u}_\nu. \tag{4.2}$$

Boundary conditions (4.2) are slightly less cumbersome than (4.1) in numerical implementation. On the other hand, usage of the thin-layer rather than the full Navier–Stokes equations enables lowering the order of the system in the streamwise direction and therefore makes the computation of the ABCs (4.1) much cheaper than the computation of the ABCs (4.2). (Indeed, the matrices $\mathbf{A}^n_k$ and $\mathbf{B}^n_k$ in (3.11), (3.12) are of order 4, whereas the same matrices constructed for the full Navier–Stokes equations [8] are of order 8.) Elimination of the resolving stage (Dirichlet-to-Neumann) also contributes essentially to the reduction of the cost of ABCs.

The questions related to the direct implementation of boundary projections for setting the ABCs are discussed in our work [29]. Here, we only present some numerical results that show high efficacy of boundary conditions (4.1) for viscous flow computations. Namely, we use the code [14, 15] to calculate a transonic turbulent flow over the airfoil RAE2822 under the nonzero angle of attack α; our treatment

TABLE 4.1

Comparison with the point-vortex (p.-v.) model for RAE2822 airfoil; $M_0 = 0.73$*;* $\mathrm{Re}_0 = 6.5 \cdot 10^6$*;* $\alpha = 2.79°$.

"Average radius" of D_{in}	2.5 chords		50 chords			
Grid	320×64		320×64		640×128	
Type of ABCs	p.-v.	(4.1)	p.-v.	(4.1)	p.-v.	(4.1)
C_l	0.8688	0.8557	0.8504	0.8492	0.8603	0.8593
Relative error	2.15%	0.42%	1.15%	1.17%	0%	0%
$C_d \times 10$	0.1123	0.1252	0.1260	0.1265	0.1255	0.1260
Relative error	10.5%	0.63%	0.40%	0.39%	0%	0%

of turbulence in the far field is based on the concept of effective viscosity and is described in [13]. Standard external boundary conditions that are incorporated in the code [14, 15] are based on the extrapolation of physical and/or characteristic variables with point-vortex enhancement. The results obtained using these standard boundary conditions are compared in Table 4.1 with the ones provided by the ABCs (4.1).

Specifically, in Table 4.1 we present the calculated values of the wave lift C_l and wave drag C_d coefficients. For a fine (640×128) grid on the big (50 chords) domain, both types of ABCs produce very close results; the corresponding values are chosen as references for calculating relative errors. For a coarser (320×64) grid on the same big domain, both types of ABCs also perform closely to one another; the discrepancy in the results between the two grids is most likely accounted for by the fact that the coarser grid is very strongly stretched. However, for the small computational domain boundary conditions, (4.1) provide much better results than the point-vortex model does. Moreover, for a 320×64 grid on the small domain the results obtained on the basis of ABCs (4.1) are clearly better than the ones obtained on the big domain for the same dimension of the grid and for both types of ABCs. This seems reasonable since on one hand the algorithm with boundary conditions (4.1) appears weakly sensitive to the size of D_{in}, and on the other hand the grid on the small domain is less stretched. Generally, the DPM-based ABCs enable one to maintain high accuracy for much smaller computational domains than standard boundary conditions do. Some other experiments show that the DPM-based ABCs may also improve the robustness of the entire algorithm.

The computational results presented above correspond to the steady-state case. However, the difference between the steady-state and the time-periodic formulations basically lies only in the number of the frequencies ω_n involved (one/more than one) and in the actual values of these frequencies (equal to zero/not equal to zero). Since for all frequencies the algorithm for calculating $\hat{\mathbf{T}}^n$ from (3.25) is the same as the one used for calculating $\mathbf{T}$ from (4.1), we expect the ABCs (3.28) to perform for the time-periodic case not worse than boundary conditions (4.1) perform for the steady-state problems.

We also note that we have described the algorithm for calculating the ABCs only for a particular class of methods used for integrating the Navier–Stokes equations inside D_{in}, namely, for such methods that the knowledge of missing relations between only two external coordinate rows of the grid (ν and ν_1) is sufficient for closing the discrete system inside the computational domain. Obviously, once the method used inside D_{in} is of higher (than the second) order, the consideration of only two curves, Γ and Γ_1, might be insufficient. However, we always can assume that the "linear region" D_{ex} contains more than one curve, e.g., Γ_1 and Γ_2 instead of only Γ_1, and can treat this case in the same way as described above. Moreover, one can use higher

order schemes for solving the linearized exterior problem as well. Such modifications may extend the possible range of applications for the technique described above by including, for example, some computational problems of aeroacoustics.

Acknowledgments. I am very thankful to V. S. Ryaben'kii of Keldysh Institute for Applied Mathematics, Russian Academy of Sciences, whose fruitful ideas constitute the foundation of our joint research in numerical methods for external problems and who influenced much of the content of this paper as well. S. Abarbanel of the School of Mathematical Sciences, Tel-Aviv University, is gratefully acknowledged for his valuable help in formulating the problem and for numerous useful discussions. I would also like to thank V. Matsaev and E. Shustin of the School of Mathematical Sciences, Tel-Aviv University, and D. Gottlieb of the Division of Applied Mathematics, Brown University, for their most helpful comments. The useful suggestions of H. Atkins, T. Roberts, and C. Swanson of NASA Langley Research Center undoubtedly contributed much to the improvement of this paper.

REFERENCES

[1] D. Givoli, *Non-reflecting boundary conditions*, J. Comput. Phys., 94 (1991), pp. 1–29.
[2] D. Givoli, *Numerical Methods for Problems in Infinite Domains*, Elsevier, Amsterdam, 1992.
[3] B. Gustafsson, *Far-field boundary conditions for time-dependent hyperbolic systems*, SIAM J. Sci. Statist. Comput., 9 (1988), pp. 812–828.
[4] B. Gustafsson, *The choice of numerical boundary conditions for hyperbolic systems*, J. Comput. Phys., 48 (1982), pp. 270–283.
[5] B. Gustafsson, *Inhomogeneous conditions at open boundaries for wave propagation problems*, Appl. Numer. Math., 4 (1988), pp. 3–19.
[6] M. H. Carpenter, D. Gottlieb, and S. Abarbanel, *Time-stable boundary conditions for finite-difference schemes solving hyperbolic systems: Methodology and application to high-order compact schemes*, J. Comput. Phys., 111 (1994), pp. 220–236.
[7] A. Seifert, A. Daraby, B. Nishri, and I. Wygnanski, *The Effects of Forced Oscillations on the Performance of Airfoils*, AIAA Paper 93–3264, AIAA Shear Flow Conference, Orlando, FL, 1993.
[8] V. S. Ryaben'kii and S. V. Tsynkov, *Artificial boundary conditions for the numerical solution of external viscous flow problems*, SIAM J. Numer. Anal., 32 (1995), pp. 1355–1389.
[9] V. S. Ryaben'kii, *Difference Potentials Method for Some Problems of Continuous Media Mechanics*, Nauka, Moscow, 1987 (in Russian).
[10] V. S. Ryaben'kii, *Boundary equations with projections*, Russian Math. Surveys, 40 (1985), pp. 147–183.
[11] V. S. Ryaben'kii, *Difference potentials method and its applications*, Math. Nachr., 177 (1996), pp. 251–264.
[12] S. V. Tsynkov, *An application of nonlocal external conditions to viscous flow computations*, J. Comput. Phys., 116 (1995), pp. 212–225.
[13] S. V. Tsynkov, E. Turkel, and S. Abarbanel, *External Flow Computations Using Global Boundary Conditions*, AIAA Journal, 34 (1996) pp. 700–706; also AIAA Paper No. 95–0562, 33rd AIAA Aerospace Sciences Meeting and Exhibit, Reno, NV, 1995.
[14] R. C. Swanson and E. Turkel, *A Multistage Time-Stepping Scheme for the Navier-Stokes Equations*, AIAA Paper 85–0035, 23rd AIAA Aerospace Sciences Meeting, Reno, NV, 1985.
[15] R. C. Swanson and E. Turkel, *Artificial Dissipation and Central Difference Schemes for the Euler and Navier-Stokes Equations*, AIAA Paper 87–1107–CP, 8th AIAA Computational Fluid Dynamics Conference, Honolulu, HI, 1987.
[16] A. Verhoff, D. Stookesberry, and S. Agrawal, *Far-field computational boundary conditions for two-dimensional external flow problems*, AIAA Journal, 30 (1992), pp. 2585–2594.
[17] A. Verhoff and D. Stookesberry, *Second-order far field computational boundary conditions for inviscid duct flow problems*, AIAA Journal, 30 (1992), pp. 1268–1276.
[18] A. Verhoff, *First-Order Far Field Computational Boundary Conditions For O-Grid Topologies*, AIAA Paper No. 95-0563, 33rd AIAA Aerospace Sciences Meeting and Exhibit, Reno, NV, 1995.
[19] V. S. Ryaben'kii, *Exact transfer of boundary conditions*, Comp. Mech. Solids, 1 (1990), pp. 129–145 (in Russian).

[20] A. P. Calderon, *Boundary-value problems for elliptic equations*, in Proc. Soviet-American Conference on Partial Differential Equations, Novosibirsk, Fizmatgiz, Moscow, 1963, pp. 303–304.
[21] D. Anderson, J. Tannehill, and R. Pletcher, *Computational Fluid Mechanics and Heat Transfer*, Hemisphere, New York, 1984.
[22] L. Hörmander, *Linear Partial Differential Operators*, Springer-Verlag, Berlin, 1963.
[23] V. S. Vladimirov, *Equations of Mathematical Physics*, Dekker, New York, 1971.
[24] S. Wolfram, *Mathematica: A System for Doing Mathematics by Computer*, Addison-Wesley, Redwood City, CA, 1991.
[25] R. Walker, *Algebraic Curves*, Princeton University Press, Princeton, NJ, 1950.
[26] B. R. Vainberg, *Some problems for hypo-elliptic equations which are well-posed in the entire plain*, Mat. Sb., 62(104) (1963), pp. 186–248 (in Russian).
[27] V. S. Ryaben'kii and S. V. Tsynkov, *An effective numerical technique for solving a special class of ordinary difference equations*, Appl. Numer. Math., 18 (1995), pp. 489–501.
[28] A. N. Kolmogorov and S. V. Fomin, *Elements of the Theory of Functions and Functional Analysis*, Nauka, Moscow, 1981 (in Russian).
[29] V. S. Ryaben'kii and S. V. Tsynkov, *An application of the difference potentials method for solving external problems in CFD*, CFD Review 1997, M. Hafez and K. Oshima, eds., John Wiley & Sons, Chichester, England, 1996.